Immunopeptidomics-based design of highly effective mRNA vaccine formulations against *Listeria monocytogenes*

Rupert L. Mayer[1,2,3], Rein Verbeke[4,5], Caroline Asselman[1,2,6], Ilke Aernout[4,5], Adillah Gul[1,2], Denzel Eggermont[1,2], Katie Boucher[1,2,3], Fabien Thery[1,2], Teresa M. Maia[3], Hans Demol[1,2,3], Ralf Gabriels[1,2], Lennart Martens[1,2], Christophe Bécavin[7], Stefaan De Smedt[4,5], Bart Vandekerckhove[5,8], Ine Lentacker[4,5], Francis Impens[1,2,3]

[1] VIB-UGent Center for Medical Biotechnology, VIB, Ghent, Belgium.

[2] Department of Biomolecular Medicine, Ghent University, Ghent, Belgium.

[3] VIB Proteomics Core, VIB, Ghent, Belgium.

[4] Ghent Research Group on Nanomedicines, Ghent University, Ghent, Belgium.

[5] Cancer Research Institute Ghent (CRIG), Ghent, Belgium.

[6] Center for Medical Genetics, Ghent University Hospital, Ghent, Belgium

[7] Université Côte d'Azur, CNRS, IPMC, Sophia-Antipolis, France.

[8] Department of Diagnostic Sciences, Ghent University, 9000 Ghent, Belgium.

Correspondence: ine.lentacker@ugent.be and francis.impens@vib-ugent.be

KEYWORDS: antigen discovery, vaccination, mass spectrometry, *Listeria monocytogenes*, bacterial infection, MHC

ABSTRACT

Listeria monocytogenes is a foodborne intracellular bacterial pathogen leading to human listeriosis. Despite a high mortality rate and increasing antibiotic resistance no clinically approved vaccine against *Listeria* is available. Attenuated *Listeria* strains offer protection and are tested as antitumor vaccine vectors, but would benefit from a better knowledge on immunodominant vector antigens. To identify novel antigens, we screened for *Listeria* epitopes presented on the surface of infected human cell lines by mass spectrometry-based immunopeptidomics. In between more than 15,000 human self-peptides, we detected 68 *Listeria* epitopes from 42 different bacterial proteins, including several known antigens. Peptide epitopes presented on different cell lines were often derived from the same bacterial surface proteins, classifying these antigens as potential vaccine candidates. Encoding these highly presented antigens in lipid nanoparticle mRNA vaccine formulations resulted in specific CD8+ T-cell responses and high levels of protection in vaccination challenge experiments in mice. Our results pave the way for the development of a clinical mRNA vaccine against *Listeria* and aid to improve attenuated *Listeria* vaccines and vectors, demonstrating the power of immunopeptidomics for next-generation bacterial vaccine development.

INTRODUCTION

Listeria monocytogenes (further referred to as *Listeria*) is a major foodborne pathogen causing listeriosis in vulnerable individuals. Infection typically occurs by consumption of contaminated food such as unpasteurized cheese or meat products [1]. The bacterium's ability to grow at refrigerator temperatures renders it a considerable risk factor in food industry and demands high levels of hygiene and monitoring [2]. Particularly for immunocompromised individuals, elderly people and pregnant women *Listeria* poses a substantial threat [3]. In severe cases the pathogen can lead to invasive gastroenteritis, sepsis, encephalitis, meningitis or endocarditis, while in pregnant women infection may lead to abortion and fetal loss [3].

After ingestion, *Listeria* can cross the intestinal barrier and via the lymph nodes enter the blood stream from where it spreads to liver and spleen [4]. Once in the bloodstream, *Listeria* may also cross the blood-brain barrier [5] or the fetoplacental barrier [6] to inflict the aforementioned complications. As a facultative intracellular pathogen, *Listeria* is capable to hide from the humoral immune system by invading host cells. The bacterium can induce its uptake in host cells via receptor-mediated endocytosis involving its surface-expressed virulence factors internalin (Inl) A and InlB [7]. Once inside the endocytic vesicle, *Listeria* secretes phospholipase (Plc) A and PlcB as well as the pore forming toxin listeriolysin O (LLO) to access the cytosol [8], where it can replicate and spread to neighboring cells via actin-based motility and expression of the actin assembly-inducing protein (ActA) at the bacterial pole [9].

While human listeriosis is not a very common type of acute infection, it has a high fatality rate of up to 30% and case numbers are gradually increasing [1]. In 2017, 2,502 cases of listeriosis were confirmed in the EU/EEA countries, while in 2007 only 1,635 cases had been reported [10-12]. In Germany the number of deceased listeriosis patients per year has risen considerably in recent years, and also more infections with antibiotic resistant *Listeria* strains have been reported [13,14]. Often resulting from local outbreaks [15-17], it was estimated that in 2010 listeriosis caused 23,150 global sicknesses leading to 5,463 deaths [18]. As *Listeria* occurs ubiquitously in the environment, domestic ruminants such as cattle, sheep and goats also get infected resulting in neurological and maternal-fetal listeriosis [19,20], hampering agricultural productivity and resulting in economic losses [21-23]. Even though cases of listeriosis are rising, no vaccines against *Listeria* are currently available or in clinical trials, presumably due to the still rather infrequent occurrence of symptomatic *Listeria* infections. Despite this restrained commercial interest to date, academic efforts to develop a safe and affordable vaccine are ongoing and could ensure the protection of vulnerable populations like pregnant women, elderly people or immunosuppressed patients [24-27]. Embracing an intracellular lifestyle, immune clearance of *Listeria* heavily relies on CD8 T cell-mediated cytotoxicity and therefore an effective vaccine must be able to induce effective cellular immunity [28]. In comparison to clinically more problematic

intracellular bacteria such as *Mycobacterium tuberculosis*, *Listeria* is relatively easy to cultivate and safe to work with and is therefore often used as a model system for intracellular bacterial infections [3].

So far mostly live attenuated vaccines against *Listeria* have been explored, typically resulting in high levels of protection in animal models [24-26,29,30]. Similarly, inactivated *Listeria* or bacterial ghosts (bacteria depleted of intracellular content) were explored as preclinical vaccine candidates [31,32]. Attenuated vaccines face a few challenges including genetic instability over extended periods of time rendering an attenuated strain more virulent again [33,34]. Next to attenuated strains, also cell-based, DNA-based, viral vector, subunit, and recombinant protein vaccines have been explored against listeriosis [35-39]. Antigens of *Listeria* that have proven to facilitate protective immunity include predominantly LLO and invasion-associated protein p60 (p60/iap), but also glyceraldehyde-3-phosphate dehydrogenase (GAPDH/gap) [38-40]. Utilizing only such a limited antigen pool is convenient as LLO and p60 are particularly well studied, but also presents with the risk of protecting only part of the population since different MHC alleles (haplotypes) might favor presentation of different epitopes and antigens. Next to preventing listeriosis, attenuated *Listeria* strains are also tested as vaccine vectors expressing cancer-associated antigens [27], and numerous clinical studies are underway utilizing *Listeria* as vector to deliver tumor antigens for treatment of malignancies such as lung, prostate, brain, cervical cancer and others [41,42]. A recent study however identified that immunodominant *Listeria* vector epitopes can strongly bind to host MHC molecules, thereby competitively inhibiting the presentation of the cargo cancer antigen and reducing the therapeutic effect [42]. Hence, knowledge about immunodominant *Listeria* epitopes could be critical to further ameliorate attenuated *Listeria* strains as cancer vaccine vectors.

The current SARS-CoV-2 pandemic has clearly demonstrated the safety and effectiveness of messenger RNA (mRNA) vaccines and confirmed their role as next generation vaccines. [43,44]. In contrast to other vaccine platforms, these vaccines contain modified mRNA encoding pathogen antigens complexed within lipid nanoparticles. The latter protects the mRNA and allows efficient uptake and translation of the encoded pathogen antigens by host cells to elicit both cellular and humoral immune responses [45]. Besides viral applications, mRNA-based vaccines hold great potential also for intracellular bacterial pathogens as safe and versatile platforms that might greatly accelerate the vaccine development and market rollout process. In contrast to viral pathogens, however, bacteria typically express several thousand proteins, which renders the task of choosing the right protein antigens for vaccination a daunting one. Despite the high potential of mRNA vaccines for (intracellular) bacteria, only a handful of studies have investigated this promising avenue to date [46-48].

Since cellular immunity and cytotoxic T cells are key to protect against intracellular pathogens, elucidating the antigens presented by MHC class I molecules on the surface of infected cells is critical for successful

vaccine development against these pathogens. This can be achieved by mass spectrometry (MS)-based immunopeptidomics, a technology originally co-developed by Donald Hunt and Hans-Georg Rammensee [49-51]. While in the early days technical limitations allowed the detection of only a handful of bacteria-derived epitopes [52,53], mass spectrometry and analysis algorithms have evolved substantially now allowing to detect dozens of bacterial epitopes in a single analysis [54-57]. None of these recent immunopeptidomics studies however investigated the MHC class I immunopeptidome of *Listeria monocytogenes*, and the list of known *Listeria* antigens is rather limited. Only 206 epitopes from 79 *Listeria* antigens are listed in the IEDB database, mainly derived from LLO (69 epitopes) and p60 (41 epitopes) as well as from plcB, gap, mpl, prfA and lmo0209 (3 epitopes each) [58]. Of these, 116 epitopes are presented on MHC class I molecules.

To extend the antigen knowledge on *Listeria* we here applied an immunopeptidomics pipeline on two infected human epithelial cell lines. In between more than 15,000 human self-epitopes we identified 68 *Listeria* epitopes from 42 different bacterial antigens. Along with several known antigens, many novel antigens were detected, often derived from the bacterial periphery. Encoding highly presented antigens as vaccine candidates in mRNA vaccine formulations significantly reduced the bacterial load in liver and spleen in a vaccination-challenge study in mice. The results of this study can be used to improve *Listeria* vaccine vectors or for further preclinical development of an mRNA vaccine against *Listeria*, acting as a blueprint for the MS-based development of mRNA vaccines against other intracellular bacterial pathogens.

RESULTS

MHC class I peptides presented on *Listeria* infected cells

To identify novel *Listeria* antigens, we isolated MHC I presented peptides from cultured human HeLa and HCT-116 cells infected or not with *Listeria monocytogenes* EGD at a multiplicity of infection (MOI) of 50. Each condition was analyzed in four biological replicates starting from 350 to 540 million cells per replicate. Isolated immunopeptides from each replicate were split to subject one half to label-free liquid chromatography-tandem mass spectrometry (LC-MS/MS) analysis, while the other half was labeled with tandem mass tags (TMT), pooled, and pre-fractionated prior to LC-MS/MS analysis (Figure 1A). TMT labeling comprises tagging of the peptides of each sample with different isobaric tags before LC-MS/MS analysis of the pooled sample, allowing relative quantification upon peptide fragmentation [59]. TMT labeling of immunopeptides has previously been shown to extend the comprehensiveness of immunopeptide identification by improving peptide ionizability and fragment ion intensity during LC-MS/MS analysis [60].

Following spectral identification with the PEAKS software and filtering for high confident hits with a false discovery rate (FDR) of 1%, in total we detected 15,766 host- and 85 *Listeria*-derived immunopeptides (Figure 1B and Supplementary Table 1). Assessment of the peptide length distribution resulted in the

expected predominance of 9mers among all identified peptides, and also a considerable proportion of 8mer, 10mer, 11mer and 12mer peptides, in line with previous reports (Figure 1C) [56,61,62]. Submission of 9mer sequences from both HeLa and HCT-116 cells to MixMHCp 2.1 resulted in the reconstitution of most cell line-specific HLA motifs (Figure 1D) [63-66]. For HeLa-cell derived immunopeptides, two out of the three expressed HLA alleles matched the reference motifs well [67]. For HCT-116 cells, five out of the six expressed HLA alleles were fully reconstituted with only HLA-C*07:01 remaining unresolved supposedly due to the typically lower expression levels of HLA-C alleles [61]. Principal component analysis of the immunopeptide intensities clearly separated the infected and uninfected replicate samples in both cell lines, indicating that *Listeria* infection has an important effect on the MHC Class I presented immunopeptidome (Figure 1E). In contrast, *Listeria* infection did not lead to detectable upregulation of MHC Class II molecules on HeLa cells (Supplementary Figure 1), together with negligible predicted binding affinities for *Listeria*-derived peptides (Supplementary Table 2) excluding significant contamination of MHC Class II-derived immunopeptides. Taken together, we identified more than 15,000 MHC class I peptides presented on *Listeria* infected cells. The peptide length distribution and clustering into expected HLA binding motifs supported *bona fide* detection of the immunopeptides and high quality of the dataset.

High confident detection of *Listeria* epitopes

Next, we compared immunopeptide abundancies between the infected samples and the uninfected controls. We used this quantitative comparison as an additional filtering step to select only high confidence *Listeria* epitopes. Indeed, bacterial immunopeptides are only expected in the infected samples, however, some of these peptides came with intensity values in the control samples suggesting they are likely false positive identifications (note that with an FDR of 1% we still expect about 160 false positive epitopes in the total dataset) or quantifications (i.e. matching of noise peaks). We therefore only selected *Listeria* peptides for further analysis that were i) quantified by the PEAKS software in at least two of the infected samples and ii) showed a higher average abundance in the infected samples compared to the uninfected control. Furthermore, *Listeria* peptide sequences were searched against the human database with all possible leucine/isoleucine permutations since leucine and isoleucine residues are virtually indistinguishable by mass spectrometry due to their identical mass. In addition, also sequences found in the human database were removed from the bacterial immunopeptide list. These filtering steps resulted in 68 high confident *Listeria* peptides originating from 42 bacterial proteins (Figure 2A, Supplementary Table 2). 58 of these peptides were predicted by NetMHCpan EL 4.1 to bind to at least one of the HLA alleles expressed on HeLa or HCT-116 cells (Figure 2B) with most peptides binding to HLA-A alleles (Supplementary Figure 2), further supporting their high confident detection [67]. Moreover, we synthesized 24 of the *Listeria*-derived immunopeptides to compare their experimentally recorded MS2 spectrum with the spectrum of their synthetic counterpart. All synthetic and experimental spectra displayed a high degree of overlap with a

Pearson correlation coefficient of >0.90, confirming correct bacterial immunopeptide identification (Figure 2C and Supplementary Figure 3).

As expected, *Listeria* peptides were amongst the most highly induced peptides presented in the infected samples (Figure 2D) and absent in the control samples as observed from their missing (or occasional noise) values in the label-free data and low intensity values in the TMT data (resulting from well-documented peptide co-isolation and ratio suppression) (Figure 2E) [68,69]. Among the *Listeria* peptides identified in this project, only VAYGRQVYL from LLO was previously reported and listed in IEDB. For two other LLO epitopes (KIDYDDEMAY and SESQLIAKFGTA), prolonged sequences (AKIDYDDEMAYS, KIDYDDEMAYSESQ, KIDYDDEMAYSESQLIAKFGTAFK, DEMAYSESQLIAKFGTAFK, SESQLIAKFGTAFK) were identified in previous MHC class II studies [70,71]. Among the protein antigens of origin, eight are described in IEDB, including many proteins from the prfA-virulence gene cluster (pVGC) such as plcA (LMON_0199) [72], hly/LLO (LMON_0200) [73], mpl (LMON_0201) [72], actA (LMON_0202) [74] and plcB (LMON_0203) [72], as well as inlB (LMON_0442) [75], gap (LMON_2470) [76] and fbaA (LMON_2571) [77]. Due to the different HLA haplotype of the two cell lines, not surprisingly there was limited overlap between both *Listeria* immunopeptide sets with only a single epitope (HLPEFTNEV) from InlB presented on both cell lines. In contrast, substantially more overlap was evident at the antigen (protein) level with seven proteins represented on both cell lines, including several of the aforementioned pVGC virulence genes (Figure 2F). Taken together, from two different infected cell lines we identified 68 MHC Class I presented epitopes from 42 *Listeria* proteins, including several previously described antigens.

Listeria antigens are often derived from the bacterial periphery

According to their predicted subcellular localization [78], the majority of the detected *Listeria* antigens is located either extracellularly or at the bacterial surface (Figure 3A). This makes these antigens more easily accessible to the host antigen processing and presentation machinery, likely explaining their overrepresentation compared to bacterial cytoplasmic antigens, as suggested previously [55,79-82]. Similarly, the cluster of orthologous groups (COG) annotation revealed cell wall/membrane biogenesis as most common COG term for identified *Listeria* antigens (Figure 3B). Mapping physical and functional associations between the identified *Listeria* antigens in the STRING database [83] yielded nine clusters of associated proteins, with the two largest clusters separating again peripheral (virulence) proteins from cytoplasmic proteins (Supplementary Figure 4).

Interestingly, more than half of the identified *Listeria* epitopes was derived from only thirteen bacterial proteins of which eleven were surface-exposed or secreted antigens (Figure 3C). Such unequal presentation suggests immunodominance of these antigens, classifying them as potential vaccine candidates [57]. From these antigens, seven were identified on both cell lines and unsurprisingly comprised several well-known

virulence factors including hly/LLO, Mpl, ActA, InlB, InlC and PlcA. In addition, elongation factor Tu (EF-Tu) and glyceraldehyde-3-phosphate dehydrogenase (gap) were highly presented. Although EF-Tu and gap are abundant cytoplasmic bacterial proteins, alternative localization of these proteins to the bacterial periphery was recently described [84-86]. Interestingly, the antigen giving rise to most presented epitopes (seven on both cell lines combined) was the rather poorly characterized oligopeptide ABC transporter, periplasmic oligopeptide-binding protein OppA (TC 3.A.1.5.1, lmon_0149 in *Listeria monocytogenes* EGD). This protein is predicted to be involved in solute transport across the plasma membrane [87], similar to four other OppA proteins in *Listeria* of which two (lmon_2272 and lmon_0134) were also picked up in our screens (Figure 3C). In conclusion, most detected *Listeria* epitopes were derived from antigens at the bacterial periphery. Highly presented antigens included major virulence factors, but also poorly characterized bacterial proteins without any known harmful activity to host cells that are therefore interesting vaccine candidates.

mRNA vaccines encoding highly presented antigens provide prophylactic protection

To test whether highly presented antigens indeed provide high levels of protective immunity, seven *Listeria* proteins represented by two or more epitopes and with no known toxicity or enzymatic activity were selected as mRNA vaccine candidates, including lmon_0149, EF-Tu and LLO (depicted in green in Figure 3C). Even though LLO naturally posseses toxicity as a pore-forming agent, we opted to select it as a vaccine candidate since it is denatured and rapidly degraded at (cytosolic) pH >6 [88]. Nevertheless, to further ensure safety of LLO as antigen we encoded the non pore-forming E262K LLO variant in our mRNA formulations [89]. Moreover, using the Vaxign2 vaccine design platform we *in silico* evaluated the selected vaccine candidates by means of reverse vaccinology, calculating Vaxign-ML scores for all candidates as well as all *Listeria monocytogenes* EGD proteins [90,91]. Vaxign-ML scoring is based on a machine learning algorithm utilizing nineteen antigen properties including immunogenicity, subcellular localization and number of transmembrane helices, amongst others [92]. Interestingly, the seven selected antigens showed superior average ranking and a significantly better average score when compared to all 42 detected antigens and to all 2,847 *Listeria monocytogenes* EGD proteins (Figure 3D-E).

We next tested the protection against *Listeria* inferred by the selected vaccine candidates in two prophylactic vaccination experiments. The seven vaccine candidates were encoded in *in vitro* transcribed N1-methylpseudouridine (m1□) modified mRNA, which was complexed within cationic liposomes and administered as a vaccine to C57BL/6J mice. To this end we made use of the galsome platform in which antigen-encoding nucleoside-modified mRNA is co-delivered in cationic liposomes together with the immunopotentiator α-galactosylceramide (α-GC) as an adjuvant [93]. Co-formulation of low amounts of the glycolipid α-GC were shown to activate invariant natural killer T (iNKT) cells resulting in elevated levels of antigen-specific cellular responses facilitating a potent adaptive immune response [28,93]. In both

experiments an ovalbumin-encoding mRNA (OVA) was included as negative control and inter-experiment reference. To test whether administration of a multi-antigen vaccine has the potential to yield higher levels of protection compared to single antigens (as recently demonstrated for SARS-Cov-2 [94,95]), in the first experiment we added a combination vaccine in which mRNA encoding LLO_E262K was combined with mRNA encoding lmon_2272 in a single formulation. In the second experiment we included an additional PBS negative control to elucidate the potential immunestimulatory effect of the galsome without pathogen-related antigens. Moreover, in this experiment we also included a positive control injecting low amounts of *Listeria monocytogenes* EGD ($1x10^4$ bacteria) instead of an mRNA vaccine. These low-dose infections result in an acute listeriosis that is easily overcome by the animals, leading to a protective adaptive immune response indicating the maximum level of protection that could potentially be reached by vaccination. In both experiments prime vaccination at day 0 was followed by an identical booster at day 14 and *Listeria* infection at day 28. Three days post-challenge the animals were sacrificed and the bacterial load in liver and spleen was assessed by counting colony-forming units (CFUs) (Figure 4A).

Mice tolerated the vaccinations well with a maximal weight loss of 2.5% on the first day after vaccination and more than 75% of mice reaching their full body weight again three days post-vaccination (Supplementary Table 3). All mice vaccinated with mRNA galsomes encoding *Listeria* antigens showed a lower bacterial burden in both spleen and liver in comparison to control vaccinations with ovalbumin (Figure 4B and Supplementary Figure 5A-B). Statistically significant reductions were observed in both organs for lmon_0149, EF-Tu and the combination vaccine (LLO_E262K + lmon_2272). Vaccination with our best presented antigen lmon_0149 resulted in a ~3 log CFU reduction in the spleen and a ~1.5 log reduction in the liver as compared to the OVA negative control, protection levels that were confirmed or even exceeded in two additional independent experiments (Supplementary Figure 5C-E). Similarly, the EF-Tu mRNA vaccine diminished the bacterial CFUs by ~2 logs in the spleen and ~4 logs in the liver. While vaccinations with LLO_E262K or lmon_2272 alone did not significantly reduce the number of *Listeria*, the combined fomulation suppressed bacterial CFUs by ~1.5 log in spleen and ~3 logs in liver, suggesting that encoding multiple bacterial antigens can provide beneficial synergistic effects. These effects are however dependent on the particular antigen combination since combining lmon_0149 with LLO_E262K in an additional independent experiment did not lead to higher levels of protection compared to lmon_0149 alone (Supplementary Figure 5E). Next to these best performing antigens, vaccination with PdhD and inlB displayed significant levels of protection only in the liver with ~1 log CFU reductions for both antigens (Figure 4B and Supplementary Figure 5A-B). The sublethal *Listeria* infection as positive control could reduce the bacterial CFUs by 3.5 and 2.5 logs in spleen and liver, respectively, confirming the expected high levels of protection. Both the OVA and the PBS negative controls resulted in comparable high bacterial counts after infection in both liver and spleen, suggesting that the utilized galsome platform alone

does not infer protection by itself, but only upon administration of pathogen-specific antigen mRNA. Interestingly, when considering all seven tested antigens we observed positive correlations (Pearson and Spearman's rank r values between 0.56 and 0.69) between the number of identified epitopes/antigen and the percentage of CFU reduction, suggesting that the number of epitopes identified in immunopeptidomics experiments can indeed be used to prioritize bacterial vaccine candidates (Figure 4C-D).

mRNA vaccination with lmon_0149 induces specific CD8+ T-cell responses

Since protective immunity against *Listeria* mainly depends on T-cell-mediated immunity [28], we next tested whether mRNA vaccination with our best presented antigen lmon_0149 induced specific CD8+ T-cell responses. To this end mice were vaccinated with mRNA galsomes encoding lmon_0149 or OVA as control. After 7 days, splenocytes were isolated and pulsed with two synthetic peptide epitopes predicted from the lmon_0149 sequence by the IEDB analysis resource tools NetMHCpan (http://tools.iedb.org/mhci/, v4.1) [67] and MHC-NP (http://tools.iedb.org/mhcnp/) [96]. YSYKFIRV was tested as best predicted epitope binding to the MHC Class I H-2-Kb allele expressed by C57BL/6J mice. We also included QVFEGLYTL as a strong predicted binder for both H-2-Db and H-2-Kb since it is identical to one of the human lmon_0149 epitopes that we picked up from HeLa cells (Figure 2E, Supplementary Table 2). Mice vaccinated with lmon_0149 showed detectable levels of IFN-y producing CD8+ T-cells to both YSYKFIRV and QVFEGLYTL, but not to SIINFEKL, a well-characterized OVA epitope (Figure 5A). In contrast, mice vaccinated with OVA strongly responded to SIINFEKL but not to YSYKFIRV and QVFEGLYTL (Figure 5B and Supplementary Figure 6A), demonstrating that mRNA vaccination with lmon_0149 induces specific CD8+ T-cell responses against this *Listeria* antigen.

Together, our data show that encoding highly presented *Listeria* antigens in mRNA vaccine formulations results in specific T-cell responses and high levels of protection in vaccination-challenge experiments in mice, indicating that immunopeptidomics holds great promise to discover novel bacterial vaccine candidates. The results presented in this study could be used to develop an effective mRNA vaccine against human or animal listeriosis and serve as a template to develop mRNA vaccines against other intracellular bacterial pathogens.

DISCUSSION

Identifying immunologically relevant antigens that are presented on host cell surfaces has been challenging for intracellular bacteria due to analytical limitations. Two decades ago, the first epitopes from intracellular bacteria were identified in an untargeted way using MS-based immunopeptidomics [52]. While initial studies only yielded a handful of pathogen-derived epitopes, technological advances now allow the detection of dozens of MHC-bound bacterial peptides presented on infected cells, recently reviewed in [57]. Translation of these MS-identified epitopes into safe, broadly applicable and effective vaccines is however lagging behind,

in part due to the long development times for classical vaccines often using inactivated or attenuated pathogens [97]. We here present a workflow for the immunopeptidomics-based development of mRNA-based vaccines against intracellular bacteria. We used *Listeria monocytogenes* as a clinically relevant bacterial model pathogen to infect HeLa and HCT-116 cells, two human epithelial cell lines, and we identified *Listeria* epitopes presented on MHC class I molecules by a hybrid MS approach, combining label-free and TMT-labeled measurements. Limited overlap of peptide identifications from label-free and TMT-labeling analyses suggests high orthogonality between the two different methods facilitating highly comprehensive immunopeptidomics screening. HeLa cells have been extensively used as an infection model in *Listeria* research and refined infection protocols are available [98-100]. In addition, HeLa cells possess limited HLA allele diversity due to loss of heterozygosity leading to the expression of only three different HLA alleles aiding in immunopeptide analysis due to reduced immunopeptide complexity. Contrastingly, HCT-116 cells have been used rarely in *Listeria* research but were chosen for their intestinal origin and epithelial morphology mimicking natural *Listeria*-targeted cells [101]. HCT-116 cells furthermore possess an HLA haplotype comprising many common HLA alleles such as HLA-A*02:01, HLA-A*01:01, HLA-C*05:01 and HLA-C*07:01 [102]. In contrast to antigen presenting cells of myeloid origin, HeLa and HCT-116 cells only express negligible levels of MHC class II [63,66]. This strongly reduced the risk of accidental co-enrichment of MHC class II ligands in our screens, although some trace contamination cannot be excluded [103]. Nevertheless, in conjunction with serial dual step immunoprecipitation strategies [56,104-106], myeloid cells could be included in future screens to complement the MHC Class I epitopes reported here with MHC Class II-presented *Listeria* epitopes.

We detected 68 high confident epitopes from 42 different *Listeria* antigens including several well-known virulence factors such as LLO, InlB and ActA, as well as previously uncharacterized proteins. One example of the latter is lmon_0149 denoted as Oligopeptide ABC transporter, periplasmic oligopeptide-binding protein OppA, which we identified as most presented antigen with 7 different epitopes detected on both cell lines. In *Listeria monocytogenes* EGD, five proteins are annotated as OppA (lmon_0149, lmon_2272, lmon_2584, lmon_0134, lmon_2115 in EGD), of which three, lmon_0149, lmon_2272 and lmon_0134, were represented by MHC Class I epitopes in our data. The homolog of lmon_2272 in *Listeria monocytogenes* EDGe (lmo0152) has been demonstrated to mediate oligopeptide transport and facilitate bacterial growth at low temperatures, while it also plays a role in intracellular and *in vivo* infection [107]. It is also involved in quorum sensing, beta-lactam resistance and acts as an ABC transporter according to the Kyoto Encyclopedia of Genes and Genomes (KEGG) [108-110]. The other four OppA proteins are less well studied, but based on structural similarities are likely also involved in solute transport across the plasma membrane [87] and regulated upon growth at low temperatures or in organs or blood [111].

The parent *Listeria* antigen proteins were ranked according to the identified epitope count and the top seven candidates devoid of any known enzymatic activity were selected as vaccine candidates. The antigen sequence information was translated into nucleoside-modified mRNA and formulated in cationic lipid nanoparticles including the glycolipid α-GC as a smart adjuvant termed galsomes. This mRNA platform facilitates a pluripotent innate and adaptive immune response spearheaded by invariant natural killer T (iNKT) cells [93]. Upon vaccination, galsomes are taken up by dendritic cells (DCs) leading to surface presentation of i) the mRNA-encoded antigens on MHC I molecules activating CD8 T cells and ii) α-GC on CD1d glycolipid receptors stimulating iNKT cells. iNKT cells can further activate DCs through CD40 ligation which enhances DC maturation thereby improving T cell activation capacity [112]. In addition, the response of iNKT cells to α-GC results in a burst release of cytokines and chemokines, which further promotes and regulates immunity [113]. Moreover, prior reports evidenced that activated NKT cells provide early protection against enteric *Listeria* infection with systemic production of IFN-γ [114].

Following prime-boost vaccination and *Listeria* challenge in mice, most antigens significantly reduced the bacterial load in the liver, while lmon_0149 and EF-Tu also showed significant protection in the spleen. Mice vaccinated with our top candidate lmon_0149 contained 1000x less bacteria in the spleen compared to OVA-vaccinated control animals. This reduction is less pronounced compared to reductions reported for live attenuated strains [27], but differences in vaccination schemes, *Listeria* strains used and infection doses make direct comparisons difficult. Most importantly, lmon_0149 vaccination resulted in a protection that was almost as high as the protection offered by a low-dose *Listeria* infection. Given the short interval between infection and organ harvest we suspect that lmon_0149 vaccinations would facilitate complete clearance given sufficient time for the immune system to completely eliminate the pathogen from the host. The specific CD8+ T-cell responses that we measured against two epitopes from lmon_0149 further indicated that vaccination induces cellular immunity, known to be required for protection against *Listeria* [28]. EF-Tu was a somewhat surprising hit as it is typically denoted as a highly abundant cytoplasmic protein functioning as elongation factor during protein biosynthesis and was therefore not expected to be readily available for host antigen processing [78,85]. However, more recent reports showcase a moonlighting function of EF-Tu as fibronectin-binding molecule at the cell surface [84,115,116], likely explaining its favorable results as a vaccine candidate and also its immunogenicity during infection with *Borrelia burgdorferi*, *Chlamydia trachomatis* and *Helicobacter pylori* [117-119]. While EF-Tu seems a promising vaccination candidate in *Listeria* offering a remarkably high (4 log) protection in the liver, it is highly conserved amongst prokaryotic species and might therefore potentially lead to autoimmune-like side effects against the host microbiome [120]. Strikingly, the combination of the two antigens LLO_E262K and LMON_2272 OppA resulted also in statistically significant and high levels of protection in both spleen and liver similar to lmon_0149, while the individual, separate vaccinations did not achieve significant levels of protection. This

hints towards a synergistic effect of this particular combination of antigens, a promising observation that warrants future testing of other antigen combinations including top candidates such as lmon_0149. An initial attempt to combine lmon_0149 vaccination with LLO_E262K did however not result in higher levels of protection compared to vaccination with lmon_0149 alone, indicating that effective combinations will be antigen-dependent. This result further highlights the surprisingly low protection offered by LLO_E262K, in contrast with many mice and human trials where epitopes within LLO have been identified as immunodominant [39,40,42,73]. We speculate that this might be related to LLO's expression as a cytosolic intracellular protein in the case of mRNA vaccination versus delivery as an extracellular antigen in the case of vaccination with a recombinant subunit or live attenuated strain. At cytosolic pH >6 LLO is denatured and rapidly degraded [88], a process that might occur with different kinetics and that may result in different epitopes for host-cell expressed LLO versus bacterially expressed or ectopically delivered LLO.

To the best of our knowledge, this is the first report describing an mRNA-based, cell-free vaccine against an intracellular bacterium demonstrating high levels of protection in vaccination-challenge experiments. Previous lipid nanoparticle mRNA vaccines against bacterial pathogens such as *Mycobacterium tuberculosis* and Group A and B *Streptococci* showed promising results, but either did not report, or reported only moderate reductions in bacterial burden upon vaccination. [46-48,121]. Recently, an mRNA vaccine encoding nineteen saliva proteins from *Ixodes scapularis* (black-legged tick) led to acquired tick resistance and reduced transmission of the Lyme disease agent *Borrelia burgdorferi* in Guinea pigs, however, in this case the vector instead of the pathogen was targeted by the vaccine [122]. It is noteworthy that despite their initial detection on infected human cells, the *Listeria* antigens identified here are also immunologically relevant for the chosen mouse model as evidenced by the vaccination-challenge experiments. These antigens therefore hold great promise for further development of *Listeria* vaccines for both human and animal use. Preclinical studies in humanized mice will help to determine the protective potential in man. Moreover, high conservation levels of the identified epitopes suggest that the current *Listeria monocytogenes* EGD-based sequences encoded in the mRNA will provide protection against a broad range of *Listeria monocytogenes* strains, including clinical and veterinary isolates (Supplementary Figure 7).

Finally, beyond the development of an anti-listeria vaccine, the encountered correlation of highly presented antigens inferring the greatest levels of protection could facilitate the process of vaccine antigen prioritization, speeding up vaccine development and preserving valuable resources in the battle against rising antimicrobial resistance (AMR) levels of bacterial pathogens. Future screens will show whether this hypothesis holds true. In this regard, the present study can act as a blueprint for immunopeptidomics-based development of mRNA vaccines against intracellular bacterial pathogens. Moreover, the *Listeria* antigens and epitopes identified here could be used to improve *Listeria* strains that are tested as cancer vaccine

vectors. Due to the preferential presentation of immunodominant *Listeria* epitopes, these vectors were recently reported to suffer from reduced efficacy in cargo antigen presentation [42]. Future efforts could attempt to delete several of the novel *Listeria* antigens reported here or to mutate their epitope anchor residues in order to abolish MHC binding and to free up presentation capacity for the actual target cancer epitopes.

Materials and Methods

Cell Culture

Human HeLa cells (ECACC 93021013), HCT-116 cells (ECACC 91091005) and JY cells (ECACC 94022533) were cultured at 37°C in a humidified atmosphere at 10% CO_2. HeLa cells were grown without antibiotics in MEM medium (#M2279, Merck) supplemented with 10% fetal bovine serum (FBS, #10270106, Thermo Fisher Scientific), 2mM GlutaMax (#35050038, Thermo Fisher Scientific), 1% non-essential amino acids (#11140035, Thermo Fisher Scientific), 1 mM sodium pyruvate (#11360039, Thermo Fisher Scientific) and 10 mM HEPES (#15630056, Thermo Fisher Scientific). HCT-116 cells were maintained without antibiotics in McCoy's 5A (modified) medium, HEPES (#22330070, Thermo Fisher Scientific) supplemented with 10% FBS and 2 mM GlutaMax. JY cells were cultured without antibiotics in RPMI medium (#61870036, Thermo Fisher Scientific) supplemented with 10% FBS and 2 mM GlutaMax. HeLa and HCT-116 cells were passaged at around 75% confluency in T175 flasks (#660160, Greiner Bio-One) and all three cell lines were tested and confirmed negative for mycoplasma contamination.

Listeria infection of HeLa and HCT-116 cells

Listeria monocytogenes EGD (BUG600 strain) was grown in brain heart infusion (BHI) broth (#10462498, Fisher Scientific) shaking at 37 °C. *Listeria* were cultured overnight and then subcultured 1:20. At a density of 1E9/ml, bacteria were washed three times with PBS (#14040-174, Life Technologies) and resuspended in HeLa or HCT-116 growth medium without FBS prior to infection at an MOI of 50. For infection, HeLa or HCT-116 cells were grown in T175 flasks to a density of 7E6 cells/flask (HeLa) and 15E6 cells/flask (HCT-116). Directly before infection, cells were washed with PBS and 20 mL bacterial inoculum was added followed by incubation for 1h at 37°C and 10% CO_2 to allow bacterial entry. Afterwards, cells were washed two times with PBS and then grown further for 23 hours in cell culture medium with 10% FBS, supplemented with 40 µg/mL of gentamicin (#G1397-10ML, Sigma-Aldrich, Merck) to kill extracellular bacteria. Cells were harvested using cell dissociation buffer (#13151-014, Life Technologies), washed three times with PBS and the dry cell pellet was stored at -80°C until further processing.

Generation of immunoaffinity columns for MHC Class I pull down

W6/32 antibody was purified from hybridoma cell (HB-95™, ATCC) supernatant as recommended by the cell line provider. Immunoaffinity columns were generated as described [123]. Briefly, 0.5 mL of precipitated protein A sepharose 4B beads (#101041, Thermo Fisher Scientific) were washed with 100 mM Tris pH 8.0 (#0210313305, MP Biomedicals) before 3 mg of purified W6/32 antibody was added and allowed to bind at room temperature for 1h in a rolling tube. W6/32-bound sepharose beads were then washed with 0.2 M sodium borate pH 9 (#B3545-500G, Sigma-Aldrich, Merck) and fresh 20 mM dimethylpimelimidate

(#D8388-250MG, Sigma-Aldrich, Merck) dissolved in sodium borate solution was added for cross-linking of the W6/32 antibody to the beads. Cross-linking occured for 30 min in a rolling tube after which beads were washed with 0.2 M ethanol amine pH 8 (#149582500, Thermo Fisher Scientific) to quench the crosslinking reaction.

Isolation and purification of immunopeptides

Cells were lysed by addition of a mild lysis buffer containing 1% octyl-β,D-glucopyranoside (#O9882-500MG, Sigma-Aldrich, Merck), 0.25% sodium deoxycholate (#1065040250, Millipore, Merck), 1.25x cOmplete protease inhibitor cocktail (#4693159001, Roche), 1 mM phenylmethylsulfonyl fluoride (#52332-5GM, Sigma-Aldrich, Merck), 0.2 mM iodoacetamide (#I1149-5G, Sigma-Aldrich, Merck) and 1 mM ethylendiamine tetraacetic acid (EDTA) (#EDS-100G, Sigma-Aldrich, Merck) in Ca/Mg-free PBS (#14190-169, Thermo Fisher Scientific). Ice cold lysis buffer was added at a ratio of 1 mL per 1E8 cells and lysis occured for 1h on ice facilitated by vortexing and pipetting up the and down the lysate every 5 min. Lysates were then cleared by initial centrifugation at 2,000 x g for 10 min at 4°C, and supernatants were further cleared at 16,100 x g for 35 min at 4°C. Prior to immunoprecipitation, W6/32 immunoaffinity columns were washed with 0.1 M acetic acid (#1000562500, Sigma-Aldrich, Merck), followed by 100 mM TRIS pH 8.

Supernatants were added to the washed W6/32 immunoaffinity columns and precipitated overnight while rolling at 30 rpm at 4°C. Reusable Econo glass columns (#7374150, Bio-Rad) were used for the immunoprecipitation. Beads were washed with ice cold solutions in the cold room: twice with 150 mM sodium chloride (#S0520, Duchefa Biochemie) in 20mM TRIS pH 8, twice with 400 mM NaCl in 20 mM TRIS pH8, again twice with 150 mM NaCl in 20 mM TRIS pH 8 and finally twice with 20 mM TRIS pH 8. MHC Class I:peptide complexes were eluted by applying 5 mL 10% acetic acid per 500 µL settled beads.

The eluate was further acidified to a final concentration of 0.5% trifluoroacetic acid (#85183, Thermo Fisher Scientific) and pH was checked to be at 2.5 or below, prior to loading on preconditioned C18 ODS 100 mg SampliQ columns (#5982-1111, Agilent Technologies) using a vacuum manifold. After initial loading, samples were re-loaded four times before washing with 1 mL of 2% acetonitrile (ACN) (#1000292500, Sigma-Aldrich, Merck) in 0.2% acetic acid. Next, MHC class I peptides were specifically eluted by applying twice 300 µL of 30% acetonitrile in 0.2% trifluoracetic acid, followed by pooling of the eluates and complete drying in 2 mL protein LoBind tubes (#0030108450, Eppendorf). For further purification, immunopeptides were reconstituted in 100 µl of 2% ACN in 0.2% TFA for 15 min in an ultrasonic bath. OMIX C18 pipette tips (#A57003MB, Agilent Technologies) were conditioned three times with 200 µl of 80% ACN in 0.2% TFA, followed by five times 200 µl of 0.2% TFA. Resolubilized MHC-peptides were loaded onto the conditioned OMIX tips by pipetting up and down ten times, washed with 100 µL of 0.2% TFA and eluted by pipetting up and down ten times with 80 µl of 30% ACN in 0.2% TFA,

followed by 20 µl of 30% ACN in 0.2% TFA. Eluates were pooled and divided in two equal fractions per sample to allow parallel label-free and TMT-labeling analysis. Both aliquots were completely dried and stored at -20°C until further use.

TMT labeling and pre-fractionation of immunopeptides

Dried immunopeptides were dissolved in 10 µl of 100 mM tetraethylammonium bicarbonate (#T7408-100ML, Sigma-Aldrich, Merck) by vortexing and sonicating for 15 minutes. TMT10plex labels (#90110, Thermo Fisher Scientific) were dissolved in 41 µl of anhydrous ACN and were regularly vortexed for 5 minutes to completely dissolve the labels. Next, 4.1 µl of TMT-label was added to each sample of peptides. For HeLa, uninfected samples 1 to 4 were labeled with the 127N, 127C, 128N and 128C TMT labels, while *Listeria* infected samples were labeled with 129N, 129C, 130N, and 130C. For HCT-116, uninfected samples 1 to 4 were labeled with 126, 127N, 127C and 128N, while *Listeria* infected samples were labeled with the 129C, 130N, 130C and 131 TMT reagents. Peptides were incubated with the TMT-labels for 1h at room temperature while shaking at 700 rpm. 1 µl of hydroxylamine (#15675820, Fluka, Thermo Fisher Scientific) was then added to quench the reaction followed by incubation for 15 min at room temperature while shaking at 700 rpm. After quenching, the TMT-labeled samples from each cell line were pooled and dried completely. The TMT-labeled and pooled immunopeptides were then separated into 12 fractions using a reversed phase C18-column at pH 10 and pH 5.5 for HeLa and HCT-116 cells, respectively. Dried peptides were solubilized in 100 µl of 2% ACN and 0.1% TFA in ultrapure water. 95 µl thereof was injected into an LC-system, consisting of a capillary pump (#G1376A, Agilent), an isocratic pump (#G1310A, Agilent), a multiple wavelength detector (#G1365B, Agilent), a column compartment (#G1316A, Agilent), a degasser (#G1379B, Agilent) and a well-plate autosampler (#G1367A, Agilent). Peptides were first loaded onto a 4 cm trapping column (made in-house, 250 µm internal diameter, 5 µm beads diameter, C18 Reprosil-HD, Dr. Maisch, Germany) at a flow rate of 25 µl/min. As mobile phase, two different solvents were used. Solvent A consisted of 10 mM ammonium bicarbonate (#09830, Sigma-Aldrich, Merck) and 2% ACN in ultrapure water while solvent B consisted of 10 mM ammonium bicarbonate and 70% ACN in ultrapure water. The pre-fractionation started with 0% B followed by a linear increase from 0% to 100% B in 100 minutes between minute 20 and 120. The gradient was followed by a stationary washing phase at 100% B for 5 minutes and re-equilibration with 0% B for 15 minutes. Eluting fractions were collected using a Probot micro-fraction collector (#161403, LC-packings) into 12 MS-vials. Fractions were collected every minute from minute 20 onwards. After the first 12 fractions were collected in vial 1 to 12, the 13th fraction was again collected in vial 1 to re-start the collection cycle and to pool fractions in a smart way ensuring homogenous distribution of peptide hydrophobicity within each MS vial. Fractions were collected for a total of 84 minutes and the fractionated samples were vacuum-dried and stored at -20°C prior to LC-MS/MS analysis.

LC-MS/MS and data analysis of immunopeptides

Purified immunopeptides for label-free analysis were redissolved in 15 µl loading solvent (0.1% trifluoroacetic acid (TFA) in water/acetonitrile (ACN) (98:2, v/v)) from which 10 µL was injected for LC-MS/MS analysis on an Ultimate 3000 RSLC nano-LC system (Thermo Fisher Scientific, Bremen, Germany) in-line connected to a Q Exactive HF mass spectrometer (Thermo Fisher Scientific) equipped with a nanospray flex ion source (Thermo Fisher Scientific). Trapping was performed at 10 µl/min for 4 min in loading solvent on a 20-mm trapping column (made in-house, 100 µm internal diameter, 5 µm beads, C18 Reprosil-HD, Dr Maisch, Ammerbuch-Entringen, Germany). Peptide separation after trapping was performed on a 200 cm micropillar array column (µPAC, PharmaFluidics) with C18-endcapped functionality. The Ultimate 3000's column oven was set to 50°C and for proper ionization a fused silica PicoTip emitter (10 µm inner diameter, New Objective, Littleton, MA, US) was connected to the µPAC outlet union and a grounded connection was provided to this union. Peptides were eluted by a non-linear gradient from 1 to 55% MS solvent B (0.1% FA in water/acetonitrile (2:8, v/v)) over 145 min, starting at a flow rate of 750 nl/min switching to 300 nl/min after 25 min, followed by a 15-min washing phase plateauing at 99% MS solvent B. Re-equilibration with 99% MS solvent A (0.1% FA in water) was performed at 300 nl/min for 45 min followed by 5 min at 750 nl/min adding up to a total run length of 210 min. The mass spectrometer was operated in data dependent, positive ionization mode, automatically switching between MS and MS/MS acquisition for the 10 most abundant peaks in a given MS spectrum. The source voltage was 2.2 kV, and the capillary temperature was set at 275 °C. One MS1 scan (m/z 300–1,650, AGC target 3×10^6 ions, maximum ion injection time 60 ms), acquired at a resolution of 60,000 (at 200 m/z), was followed by up to 10 tandem MS scans (resolution 15,000 at 200 m/z) of the most intense ions fulfilling predefined selection criteria (AGC target 1×10^5 ions, maximum ion injection time 120 ms, isolation window 1.5 Da, fixed first mass 100 m/z, spectrum data type: centroid, intensity threshold 8.3×10^3, exclusion of unassigned, 4-8, >8 positively charged precursors, peptide match off, exclude isotopes on, dynamic exclusion time 12 s). The higher-energy collisional dissociation was set to 28% normalized collision energy, and the polydimethylcyclosiloxane background ion at 445.12003 Da was used for internal calibration (lock mass).

Fractionated and TMT-labeled immunopeptides were redissolved in 20 µl loading solvent from which 15 µL was injected for LC-MS/MS analysis on an Ultimate 3000 RSLC nano-LC system (Thermo Fisher Scientific, Bremen, Germany) in-line connected to a Fusion Lumos mass spectrometer (Thermo Fisher Scientific). Trapping was performed as described above and peptides were again separated on a 200 cm-long micropillar array column (µPAC, PharmaFluidics) with C18-endcapped functionality. Peptides were eluted by a non-linear gradient from 1 to 55% MS solvent B over 87 min, starting at a flow rate of 750 nl/min switching to 300 nl/min after 15 min, followed by a 13-min washing phase plateauing at 99%

MS solvent B. Re-equilibration with 99% MS solvent A was performed at 300 nl/min for 40 min adding up to a total run length of 140 min. The mass spectrometer was operated in data dependent, positive ionization mode, automatically switching between MS and MS/MS acquisition to enable a cycle time of 3 s. One MS1 scan (m/z 300–1,650, AGC target 4×10^5 ions, maximum ion injection time 50 ms), acquired at a resolution of 120,000 (at 200 m/z), was followed by tandem MS scans in the orbitrap (resolution 50,000 at 200 m/z) of the most intense ions fulfilling predefined selection criteria (AGC target 7.5×10^4 ions, maximum ion injection time 120 ms, isolation window 1 Da, fixed first mass 100 m/z, spectrum data type: centroid, intensity threshold 8.3×10^3, including, 2-5 positively charged precursors, peptide match off, exclude isotopes on, dynamic exclusion time 60 s). The higher-energy collisional dissociation (HCD) was set to 38% normalized collision energy, and the polydimethylcyclosiloxane background ion at 445.12003 Da was used for internal calibration (lock mass).

Mass spectrometry raw data were searched with PEAKS Studio X (Bioinformatics Solutions Inc, Waterloo, Canada) against a database of the human sequences in Uniprot SwissProt (version January 2019, 20,413 entries) merged with *Listeria monocytogenes* EGD sequences from TrEMBL (version April 2019, 2,847 entries) [124]. Databases were merged using dbtoolkit 2.0 (version 4.2.5) [125]. The peptide length was restricted to 8-30 amino acids, and unspecific digestion was chosen as digest mode. Methionine oxidation and N-terminal acetylation were set as variable modifications, and mass error tolerances were set to 10 ppm and 0.02 Da for parent and fragment ions, respectively. For indicating potential contaminant peptides, the MaxQuant contaminant database (MQ version 1.6.3.4) was enabled [126]. False discovery rate (FDR) estimation was carried out using the decoy-fusion approach. Identified peptide sequences were filtered at the PSM level for an FDR of 1% or better prior to label-free or TMT-10plex quantification in PEAKS Studio. Quantification results were not filtered and TMT-labeled peptide quantifications not normalized before export as csv files for further processing using the Perseus software platform [127]. Exported csv files for label-free and TMT-labeled data were loaded into Perseus separately and intensity values were $\log_2$ transformed. After categorical annotation into uninfected, healthy and *Listeria*-infected sample groups, the data was filtered for at least two valid values in at least one sample group. Missing values were imputed from a normal distribution around the detection limit and a principal component analysis (PCA) was performed. Volcano plots were generated by plotting the results of a two-sided Student's t-test of *Listeria*-infected against uninfected samples employing permutation-based multiparameter correction at an FDR of 5%. Heat maps were constructed by z-scoring *Listeria*-derived peptide $\log_2$ intensities before hierarchical clustering.

Calculation of correlation coefficients between *Listeria*-derived and synthetic peptides

Python 3.7 was used to calculate spectral correlation including spectrum_utils version 0.3.5 and pyteomics version 4.5.2 [128,129]. Spectrum processing was performed by annotation of fragment ion peaks for a, b and y ions including singly and doubly charged ions, followed by removal of precursor peaks for up to two isotopes and removal of low intensity (<5% of the maximum) peaks. All steps used a 50 ppm mass error tolerance. Pearson correlations were calculated on the intensities of all annotated fragment ions per spectrum. The code including an example peptide can be found on GitHub (https://github.com/RalfG/2022-listeria-spectrum-similarity) and Zenodo (https://doi.org/10.5281/zenodo.5948475). A runnable version of the script can be found online at Binder (https://mybinder.org/v2/gh/RalfG/2022-listeria-spectrum-similarity/HEAD?labpath=2022-listeria-spectrum-similarity.ipynb).

mRNA production and liposome vaccine formulation

The protein sequences of the selected seven *Listeria* genes were cloned into a pGEM4z-plasmid vector (Promega) containing a T7 promoter, 5′ and 3′ UTR of human β globulin, and a poly(A) tail by Genscript. The *Listeria monocytogenes* EGD protein sequences were retrieved from the Listeriomics platform [130], codon optimized for mouse using the IDT codon optimization tool, and the final plasmid product was confirmed by sequencing. For the IVT mRNA production, plasmids were linearized with PstI (New England Biolabs, MA, USA) and purified using a PCR purification kit (Roche, Upper Bavaria, Germany). Linearized plasmids were used as templates for the in vitro transcription reaction using the T7 MegaScript kit, including an Anti-Reverse Cap Analog (ARCA, Trilink BioTechnologies), and chemically modified N1-methylpseudouridine-5'-triphosphate (Trilink BioTechnologies) instead of the normal nucleotide, uridine. The resulting capped mRNAs were purified by DNase I digestion, precipitated with LiCl and washed with 70% ethanol. All mRNAs were analysed by agarose gel electrophoresis and concentrations were determined by measuring the absorbance at 260 nm. mRNAs were stored in small aliquots at −80 °C at a concentration of 1 μg/μL.

The mRNA constructs encoding the different *Listeria* antigens were formulated in cationic liposomes containing the immunopotentiator α-galactosylceramide (α-GC), as described previously [93]. DOTAP (1,2-dioleoyl-3-trimethylammonium-propane), cholesterol, and α-GC were purchased from Avanti Polar Lipids (Alabaster, USA). Cationic liposomes of DOTAP-cholesterol (2:3 molar ratio) were prepared by the thin-film hydration method. The appropriate amounts of lipids, dissolved in chloroform were transferred into a round-bottom flask. For the incorporation of the glycolipid antigen, 0.015 mol % of the total lipid amount was replaced by α-GC. The chloroform was evaporated under nitrogen, after which the lipid film was rehydrated in HEPES buffer (20 mM, pH 7.4, Sigma-Aldrich) to obtain a final lipid concentration of 12.5 mM. The resulting cationic liposomes were sonicated in a bath sonicator (Branson Ultrasonics, Dansbury, CT, USA). Then, they were mixed with mRNA to obtain mRNA lipoplexes at a cationic lipid-to-mRNA

(N/P) ratio of 3, in a final formulation of an isotonic HEPES buffer containing 5% glucose (Sigma-Aldrich). The cationic lipoplex formulations were subjected to a size and zeta potential quality control using a Malvern Zetasizer nano-ZS (Malvern Instruments Ltd., Worcestershire, UK).

Mouse housing, prime-boost vaccination and *Listeria* infection

The animals were housed in a temperature- (21□°C) and humidity- (60%) controlled environment with 12□h light/dark cycles; food and water were provided ad libitum. The animal facility operates under the Flemish Government License Number LA1400536. All experiments were done under conditions specified by law and authorized by the Institutional Ethical Committee on Experimental Animals. *Listeria monocytogenes* (EGD BUG600 strain) was grown in brain heart infusion (BHI) medium at 37°C. Bacteria were cultured overnight and then sub cultured 1:10 in BHI medium for 2 h at 37°C. Bacteria were washed three times in PBS and resuspended in PBS at $7.5x10^5$ bacteria per 100 µl (~3x the LD50 of EGD [131]) or further diluted to 10^4 bacteria per 100 µl. Female C57BL/6 mice (Charles River Laboratories, France) at 7 weeks of age were vaccinated intravenously (i.v.) by tail vein injection with either mRNA galsomes (10 µg mRNA, total volume 100 µl in isotonic HEPES-buffered glucose solution), a sublethal dose of *Listeria monocytogenes* (1 x 10^4 bacteria in 100 µl PBS), or PBS (100µl) at day 0 and day 14 of the experiment. Combination vaccines were administered by mixing the respective ready-to-use mRNA galsomes 1+1 resulting in the administration of 5 µg mRNA for both antigens. Mouse body weight was monitored for 72 h post vaccination to assess potential adverse vaccination reactions. On day 28, the mice were infected intravenously by tail vein injection with 7.5×10^5 bacteria per animal. Mice were sacrificed 72 h following infection. Colony Forming Units (CFUs) per organ (liver or spleen) were enumerated by serial dilutions and plating on BHI agar after tissue dissociation in sterile saline. For tissue dissociation, cell strainers and PBS were employed for spleens, while livers were disintegrated using PBS with 2% tween.

Measurement of T-cell responses

Female C57BL/6 mice were intravenously injected with galsomes containing mRNA encoding the lmon_0149 antigen or ovalbumin (10 µg mRNA, 10 mice/group) or with PBS (100 µl). On day 8, 2 x 10^6 splenocytes from each animal were transferred in a round bottom 96 well plate (200 µl volume) and ex vivo restimulated with 1 µg/ml of the lmon_0149 peptides YSYKFIRV (GenScript) and QVFEGLYTL (made in house by solid phase synthesis) or the OVA-derived peptide SIINFEKL (Eurogentec, Seraing, Belgium) as control in the presence of a protein transport inhibitor cocktail of Brefeldin A and Monensin (eBioscience). Following 37°C incubation for 5 hours, cells were stained with fixable viability dye Aqua (Thermo Scientific), incubated with Fc block (CD16/32) to block nonspecific FcR binding (BD Biosciences, Erembodegem, Belgium), and surface stained with antibody CD8a (53-6.7) APC (Figure 5) or with

antibody CD8a (53-6.7) FITC and TCRbeta (H57-597)APC (Supplementary Figure 6). Cells were then fixed and permeabilized with BDCytoFix/CytoPerm solution (BD), intracellular staining using a IFN-□ (XMG1.2) PE antibody (Biolegend, San Diego, CA, USA) was performed in Cytoperm buffer for 30 min at RT. After additional washing steps, samples were measured by a MACSQuant 18 (Figure 5) or 16 (Supplementary Figure 6) flow cytometer and analysed by FlowJo® software (BD company). Three spleen samples from lmon_0149 vaccinated mice (Figure 5) and two spleen samples from PBS vaccinated mice that showed a cell viability lower than 35% were excluded from the analysis. The gating strategy is outlined in Supplementary Figure 6.

Monitoring MHC expression by western blotting and flow cytometry

HeLa and JY cells were grown in a 6 well-plate to a density of 0.5 E6 cells/well and infected with *Listeria* for 24 hours at an MOI of 25, treated with 10 ng/mL interferon-γ (#11343536, Immunotools) for 48 h or left untreated. For western blotting, cells were lysed in 1x Laëmmli buffer containing 62.5 mM Tris-HCl pH 6.8, 2% SDS, 10% glycerol, 0,005% Bromophenol blue (#J63615, Alfa Aesar) supplemented with 20 mM DTT (#D0632, Merck). Protein samples were boiled for 10 minutes at 95°C and sonicated prior to SDS-PAGE. Samples were loaded on 4-15% polyacrylamide gradient gels (#M41215, Genescript) according to the guidelines of the manufacturer. Proteins were transferred to PVDF membrane (#IPFL00010, Merck) for 30 minutes at 100 V with Tris/Boric buffer at 50 mM/50 mM. Membranes were blocked for 1 hour at room temperature (RT) with blocking buffer (#927-50000, LI-COR) and incubated with primary antibodies overnight at 4 °C diluted to 1:1,000 in TBS. The following primary antibodies were used: anti-HLA-ABC (#15240-1-AP, Proteintech), anti-HLA-DM (#21704-1-AP, Proteintech), anti-HLA-DR (#15862-1-AP, Proteintech), anti-α-tubulin (#sc-5286, Santa Cruz Biotechnology), anti-Listeriolysin O (LLO) (#ab200538, Abcam) and anti-STAT1 (#sc-464, Santa Cruz Biotechnology). The next day, membranes were washed three times for 15 minutes with TBS-Tween 0.1% (v/v) buffer and further incubated at RT for 1 h with the appropriate secondary antibody diluted to 1:5,000 (anti-mouse # 926-32210 or anti-rabbit # 926-32211, Li-COR). Membranes were washed twice with TBS-tween 0.1% (TBS-T) and once with TBS prior to detection. Immunoreactive bands were visualized on a LI-COR-Odyssey infrared scanner (Li-COR). For flow cytometry analysis, cells were first stained with fixable viability dye Zombie green (#423111, Biolegend, San Diego) and then incubated with Fc block TruStain FcX (CD16/32) to block nonspecific FcR binding (#422302, Biolegend). To detect MHC-I and MHC-II, cells were stained with antibodies against HLA-ABC (W6/32) PE (#311405, Biolegend) and HLA-DR/DP/DQ (Tü39)-APC (#361713, Biolegend), respectively. Cells were fixed with 4% PFA for 40 min (#15710, Laborimpex). Samples were measured by the MACSQuant Analyzer 16 (Miltenyi Biotec, Gladbach) and analyzed by FlowJo® software (BD Biosciences, Erembodegem). The gating strategy is outlined in Supplementary Figure 1C.

Statistics and reproducibility

Statistical tests, significant p values and number of replicates are indicated in the figure legends and are briefly described here. Immunopeptidomics experiments were performed with 4 biological replicates. Mouse vaccination-challenge experiments were performed with 5 animals/group, while mouse vaccination experiments to monitor T-cell responses were performed with 10 animals/group. Nonparametric Mann–Whitney, paired Student t, Shapiro-Wilk and Wilcoxon matched-pairs signed rank tests were performed using GraphPad Prism 9.3. P-value thresholds used for the statistical tests corresponds to * $p < 0.05$, ** $p < 0.01$, *** $p < 0.001$ and **** $p < 0.0001$. The values of single data points and the exact p-values are indicated in the source data.

DATA AVAILABILITY

The mass spectrometry proteomics data have been deposited to the ProteomeXchange Consortium via the PRIDE [132] partner repository with the dataset identifier PXD031451. Data supporting the findings of this manuscript are available within the article, the Supplementary Information and the Source Data files or are available from the corresponding authors upon reasonable request. A reporting summary for this article is available as a Supplementary information file. Source data are provided with this paper.

References

1 Smith, A. M. *et al.* Outbreak of Listeria monocytogenes in South Africa, 2017-2018: Laboratory Activities and Experiences Associated with Whole-Genome Sequencing Analysis of Isolates. *Foodborne Pathog Dis* **16**, 524-530, doi:10.1089/fpd.2018.2586 (2019).

2 Jemmi, T. & Stephan, R. Listeria monocytogenes: food-borne pathogen and hygiene indicator. *Rev Sci Tech* **25**, 571-580 (2006).

3 Radoshevich, L. & Cossart, P. Listeria monocytogenes: towards a complete picture of its physiology and pathogenesis. *Nat Rev Microbiol* **16**, 32-46, doi:10.1038/nrmicro.2017.126 (2018).

4 Daniels, J. J., Autenrieth, I. B. & Goebel, W. Interaction of Listeria monocytogenes with the intestinal epithelium. *FEMS Microbiol Lett* **190**, 323-328, doi:10.1111/j.1574-6968.2000.tb09306.x (2000).

5 Drevets, D. A. & Bronze, M. S. Listeria monocytogenes: epidemiology, human disease, and mechanisms of brain invasion. *FEMS Immunol Med Microbiol* **53**, 151-165, doi:10.1111/j.1574-695X.2008.00404.x (2008).

6 Lecuit, M. *et al.* Targeting and crossing of the human maternofetal barrier by Listeria monocytogenes: role of internalin interaction with trophoblast E-cadherin. *Proceedings of the National Academy of Sciences of the United States of America* **101**, 6152-6157, doi:10.1073/pnas.0401434101 (2004).

7 Dramsi, S., Lebrun, M. & Cossart, P. Molecular and genetic determinants involved in invasion of mammalian cells by Listeria monocytogenes. *Current topics in microbiology and immunology* **209**, 61-77 (1996).

8 Hamon, M. A., Ribet, D., Stavru, F. & Cossart, P. Listeriolysin O: the Swiss army knife of Listeria. *Trends in microbiology* **20**, 360-368, doi:10.1016/j.tim.2012.04.006 (2012).

9 Theriot, J. A., Mitchison, T. J., Tilney, L. G. & Portnoy, D. A. The rate of actin-based motility of intracellular Listeria monocytogenes equals the rate of actin polymerization. *Nature* **357**, 257-260, doi:10.1038/357257a0 (1992).

10 Control, E. C. f. D. P. a. Listeriosis. In: ECDC. Annual epidemiological report for 2017. (ECDC, Stockholm, 2020).

11 European Food Safety, A., European Centre for Disease, P. & Control. The European Union summary report on trends and sources of zoonoses, zoonotic agents and food-borne outbreaks in 2017. *EFSA J* **16**, e05500, doi:10.2903/j.efsa.2018.5500 (2018).

12 Control, E. C. f. D. P. a. Annual Epidemiological Report on Communicable Diseases in Europe 2009. (European Centre for Disease Prevention and Control, Stockholm, 2009).

13 Wilking, H. *et al.* Ongoing High Incidence and Case-Fatality Rates for Invasive Listeriosis, Germany, 2010-2019. *Emerg Infect Dis* **27**, 2485-2488, doi:10.3201/eid2709.210068 (2021).

14 Olaimat, A. N. *et al.* Emergence of Antibiotic Resistance in Listeria monocytogenes Isolated from Food Products: A Comprehensive Review. *Compr Rev Food Sci Food Saf* **17**, 1277-1292, doi:10.1111/1541-4337.12387 (2018).

15 McCollum, J. T. *et al.* Multistate outbreak of listeriosis associated with cantaloupe. *N Engl J Med* **369**, 944-953, doi:10.1056/NEJMoa1215837 (2013).

16 Halbedel, S. *et al.* Large Nationwide Outbreak of Invasive Listeriosis Associated with Blood Sausage, Germany, 2018-2019. *Emerg Infect Dis* **26**, 1456-1464, doi:10.3201/eid2607.200225 (2020).

17 Thomas, J. *et al.* Outbreak of Listeriosis in South Africa Associated with Processed Meat. *N Engl J Med* **382**, 632-643, doi:10.1056/NEJMoa1907462 (2020).

18 de Noordhout, C. M. *et al.* The global burden of listeriosis: a systematic review and meta-analysis. *Lancet Infect Dis* **14**, 1073-1082, doi:10.1016/S1473-3099(14)70870-9 (2014).

19 Brugère-Picoux, J. Ovine listeriosis. *Small Rumin. Res.*, doi:10.1016/j.smallrumres.2007.12.022 (2008).
20 Oevermann, A., Zurbriggen, A. & Vandevelde, M. Rhombencephalitis Caused by Listeria monocytogenes in Humans and Ruminants: A Zoonosis on the Rise? *Interdiscip Perspect Infect Dis* **2010**, 632513, doi:10.1155/2010/632513 (2010).
21 Mohammed, H. O. *et al.* Identification of potential on-farm sources of Listeria monocytogenes in herds of dairy cattle. *Am J Vet Res* **70**, 383-388, doi:10.2460/ajvr.70.3.383 (2009).
22 Vazquez-Boland, J. A. *et al.* Epidemiologic investigation of a silage-associated epizootic of ovine listeric encephalitis, using a new Listeria-selective enumeration medium and phage typing. *Am J Vet Res* **53**, 368-371 (1992).
23 Nightingale, K. K. *et al.* Ecology and transmission of Listeria monocytogenes infecting ruminants and in the farm environment. *Appl Environ Microbiol* **70**, 4458-4467, doi:10.1128/AEM.70.8.4458-4467.2004 (2004).
24 Darji, A., Mohamed, W., Domann, E. & Chakraborty, T. Induction of immune responses by attenuated isogenic mutant strains of Listeria monocytogenes. *Vaccine* **21 Suppl 2**, S102-109, doi:10.1016/s0264-410x(03)00208-1 (2003).
25 McLaughlin, H. P., Bahey-El-Din, M., Casey, P. G., Hill, C. & Gahan, C. G. M. A mutant in the Listeria monocytogenes Fur-regulated virulence locus (frvA) induces cellular immunity and confers protection against listeriosis in mice. *J Med Microbiol* **62**, 185-190, doi:10.1099/jmm.0.049114-0 (2013).
26 Mohamed, W., Sethi, S., Tchatalbachev, S., Darji, A. & Chakraborty, T. Protective immunity to Listeria monocytogenes infection mediated by recombinant Listeria innocua harboring the VGC locus. *PLoS One* **7**, e35503, doi:10.1371/journal.pone.0035503 (2012).
27 Hanson, W. G. *et al.* A Potent and Effective Suicidal Listeria Vaccine Platform. *Infect Immun* **87**, doi:10.1128/IAI.00144-19 (2019).
28 Pamer, E. G. Immune responses to Listeria monocytogenes. *Nat Rev Immunol* **4**, 812-823, doi:10.1038/nri1461 (2004).
29 Dowd, G. C. *et al.* Listeria monocytogenes mutants defective in gallbladder replication represent safety-enhanced vaccine delivery platforms. *Hum Vaccin Immunother* **12**, 2059-2063, doi:10.1080/21645515.2016.1154248 (2016).
30 Meng, F. *et al.* A Cross-Protective Vaccine Against 4b and 1/2b Listeria monocytogenes. *Front Microbiol* **11**, 569544, doi:10.3389/fmicb.2020.569544 (2020).
31 Wu, X. *et al.* Production of Bacterial Ghosts from Gram-Positive Pathogen Listeria monocytogenes. *Foodborne Pathog Dis* **14**, 1-7, doi:10.1089/fpd.2016.2184 (2017).
32 Rocha, C. E. V. *et al.* Alginate-chitosan microcapsules improve vaccine potential of gamma-irradiated Listeria monocytogenes against listeriosis in murine model. *Int J Biol Macromol* **176**, 567-577, doi:10.1016/j.ijbiomac.2021.02.056 (2021).
33 Nkowane, B. M. *et al.* Vaccine-associated paralytic poliomyelitis. United States: 1973 through 1984. *JAMA* **257**, 1335-1340 (1987).
34 Kew, O. *et al.* Outbreak of poliomyelitis in Hispaniola associated with circulating type 1 vaccine-derived poliovirus. *Science* **296**, 356-359, doi:10.1126/science.1068284 (2002).
35 Fensterle, J., Grode, L., Hess, J. & Kaufmann, S. H. Effective DNA vaccination against listeriosis by prime/boost inoculation with the gene gun. *J Immunol* **163**, 4510-4518 (1999).
36 Kono, M. *et al.* Enhancement of protective immunity against intracellular bacteria using type-1 polarized dendritic cell (DC) vaccine. *Vaccine* **30**, 2633-2639, doi:10.1016/j.vaccine.2012.02.026 (2012).
37 Jensen, S. *et al.* Adenovirus-based vaccine against Listeria monocytogenes: extending the concept of invariant chain linkage. *J Immunol* **191**, 4152-4164, doi:10.4049/jimmunol.1301290 (2013).

38 Calderon-Gonzalez, R. *et al.* GNP-GAPDH1-22 nanovaccines prevent neonatal listeriosis by blocking microglial apoptosis and bacterial dissemination. *Oncotarget* **8**, 53916-53934, doi:10.18632/oncotarget.19405 (2017).

39 Phelps, C. C. *et al.* A listeriolysin O subunit vaccine is protective against Listeria monocytogenes. *Vaccine* **38**, 5803-5813, doi:10.1016/j.vaccine.2020.06.049 (2020).

40 Luo, X. & Cai, X. A combined use of autolysin p60 and listeriolysin O antigens induces high protective immune responses against Listeria monocytogenes infection. *Curr Microbiol* **65**, 813-818, doi:10.1007/s00284-012-0238-9 (2012).

41 Flickinger, J. C., Jr., Rodeck, U. & Snook, A. E. Listeria monocytogenes as a Vector for Cancer Immunotherapy: Current Understanding and Progress. *Vaccines (Basel)* **6**, doi:10.3390/vaccines6030048 (2018).

42 Flickinger, J. C., Jr. *et al.* T-Cell Responses to Immunodominant Listeria Epitopes Limit Vaccine-Directed Responses to the Colorectal Cancer Antigen, Guanylyl Cyclase C. *Front Immunol* **13**, 855759, doi:10.3389/fimmu.2022.855759 (2022).

43 Baden, L. R. *et al.* Efficacy and Safety of the mRNA-1273 SARS-CoV-2 Vaccine. *N Engl J Med* **384**, 403-416, doi:10.1056/NEJMoa2035389 (2021).

44 Polack, F. P. *et al.* Safety and Efficacy of the BNT162b2 mRNA Covid-19 Vaccine. *N Engl J Med* **383**, 2603-2615, doi:10.1056/NEJMoa2034577 (2020).

45 Reichmuth, A. M., Oberli, M. A., Jaklenec, A., Langer, R. & Blankschtein, D. mRNA vaccine delivery using lipid nanoparticles. *Ther Deliv* **7**, 319-334, doi:10.4155/tde-2016-0006 (2016).

46 Lorenzi, J. C. *et al.* Intranasal vaccination with messenger RNA as a new approach in gene therapy: use against tuberculosis. *BMC Biotechnol* **10**, 77, doi:10.1186/1472-6750-10-77 (2010).

47 Maruggi, G. *et al.* Immunogenicity and protective efficacy induced by self-amplifying mRNA vaccines encoding bacterial antigens. *Vaccine* **35**, 361-368, doi:10.1016/j.vaccine.2016.11.040 (2017).

48 Xue, T. *et al.* RNA encoding the MPT83 antigen induces protective immune responses against Mycobacterium tuberculosis infection. *Infect Immun* **72**, 6324-6329, doi:10.1128/IAI.72.11.6324-6329.2004 (2004).

49 Hunt, D. F. *et al.* Characterization of peptides bound to the class I MHC molecule HLA-A2.1 by mass spectrometry. *Science* **255**, 1261-1263 (1992).

50 Falk, K., Rotzschke, O., Stevanovic, S., Jung, G. & Rammensee, H. G. Allele-specific motifs revealed by sequencing of self-peptides eluted from MHC molecules. *Nature* **351**, 290-296, doi:10.1038/351290a0 (1991).

51 Schirle, M. *et al.* Identification of tumor-associated MHC class I ligands by a novel T cell-independent approach. *Eur J Immunol* **30**, 2216-2225, doi:10.1002/1521-4141(2000)30:8<2216::AID-IMMU2216>3.0.CO;2-7 (2000).

52 Flyer, D. C. *et al.* Identification by mass spectrometry of CD8(+)-T-cell Mycobacterium tuberculosis epitopes within the Rv0341 gene product. *Infect Immun* **70**, 2926-2932, doi:10.1128/iai.70.6.2926-2932.2002 (2002).

53 Karunakaran, K. P. *et al.* Immunoproteomic discovery of novel T cell antigens from the obligate intracellular pathogen Chlamydia. *J Immunol* **180**, 2459-2465, doi:10.4049/jimmunol.180.4.2459 (2008).

54 Karunakaran, K. P. *et al.* Identification of MHC-Bound Peptides from Dendritic Cells Infected with Salmonella enterica Strain SL1344: Implications for a Nontyphoidal Salmonella Vaccine. *J Proteome Res* **16**, 298-306, doi:10.1021/acs.jproteome.6b00926 (2017).

55 Graham, D. B. *et al.* Antigen discovery and specification of immunodominance hierarchies for MHCII-restricted epitopes. *Nat Med* **24**, 1762-1772, doi:10.1038/s41591-018-0203-7 (2018).

56 Bettencourt, P. *et al.* Identification of antigens presented by MHC for vaccines against tuberculosis. *NPJ Vaccines* **5**, 2, doi:10.1038/s41541-019-0148-y (2020).
57 Mayer, R. L. & Impens, F. Immunopeptidomics for next-generation bacterial vaccine development. *Trends Microbiol*, doi:10.1016/j.tim.2021.04.010 (2021).
58 Vita, R. *et al.* The Immune Epitope Database (IEDB): 2018 update. *Nucleic Acids Res* **47**, D339-D343, doi:10.1093/nar/gky1006 (2019).
59 Thompson, A. *et al.* Tandem mass tags: a novel quantification strategy for comparative analysis of complex protein mixtures by MS/MS. *Anal Chem* **75**, 1895-1904 (2003).
60 Pfammatter, S. *et al.* Extending the Comprehensiveness of Immunopeptidome Analyses Using Isobaric Peptide Labeling. *Analytical chemistry* **92**, 9194-9204, doi:10.1021/acs.analchem.0c01545 (2020).
61 Bassani-Sternberg, M., Pletscher-Frankild, S., Jensen, L. J. & Mann, M. Mass spectrometry of human leukocyte antigen class I peptidomes reveals strong effects of protein abundance and turnover on antigen presentation. *Mol Cell Proteomics* **14**, 658-673, doi:10.1074/mcp.M114.042812 (2015).
62 Marcu, A. *et al.* HLA Ligand Atlas: a benign reference of HLA-presented peptides to improve T-cell-based cancer immunotherapy. *J Immunother Cancer* **9**, doi:10.1136/jitc-2020-002071 (2021).
63 Scholtalbers, J. *et al.* TCLP: an online cancer cell line catalogue integrating HLA type, predicted neo-epitopes, virus and gene expression. *Genome Med* **7**, 118, doi:10.1186/s13073-015-0240-5 (2015).
64 Bassani-Sternberg, M. & Gfeller, D. Unsupervised HLA Peptidome Deconvolution Improves Ligand Prediction Accuracy and Predicts Cooperative Effects in Peptide-HLA Interactions. *J Immunol* **197**, 2492-2499, doi:10.4049/jimmunol.1600808 (2016).
65 Gfeller, D. *et al.* The Length Distribution and Multiple Specificity of Naturally Presented HLA-I Ligands. *J Immunol* **201**, 3705-3716, doi:10.4049/jimmunol.1800914 (2018).
66 Boegel, S., Lower, M., Bukur, T., Sahin, U. & Castle, J. C. A catalog of HLA type, HLA expression, and neo-epitope candidates in human cancer cell lines. *Oncoimmunology* **3**, e954893, doi:10.4161/21624011.2014.954893 (2014).
67 Reynisson, B., Alvarez, B., Paul, S., Peters, B. & Nielsen, M. NetMHCpan-4.1 and NetMHCIIpan-4.0: improved predictions of MHC antigen presentation by concurrent motif deconvolution and integration of MS MHC eluted ligand data. *Nucleic Acids Res* **48**, W449-W454, doi:10.1093/nar/gkaa379 (2020).
68 Ow, S. Y. *et al.* iTRAQ underestimation in simple and complex mixtures: "the good, the bad and the ugly". *J Proteome Res* **8**, 5347-5355, doi:10.1021/pr900634c (2009).
69 Savitski, M. M. *et al.* Measuring and managing ratio compression for accurate iTRAQ/TMT quantification. *J Proteome Res* **12**, 3586-3598, doi:10.1021/pr400098r (2013).
70 Paschen, A. *et al.* Identification of a cross-reactive HLA-DRB1*0301-restricted CD4 T cell response directed against cholesterol-binding cytolysins from two different pathogens. *Microbes Infect* **8**, 2034-2043, doi:10.1016/j.micinf.2006.03.010 (2006).
71 Safley, S. A., Jensen, P. E., Reay, P. A. & Ziegler, H. K. Mechanisms of T cell epitope immunodominance analyzed in murine listeriosis. *J Immunol* **155**, 4355-4366 (1995).
72 Busch, D. H., Bouwer, H. G., Hinrichs, D. & Pamer, E. G. A nonamer peptide derived from Listeria monocytogenes metalloprotease is presented to cytolytic T lymphocytes. *Infect Immun* **65**, 5326-5329, doi:10.1128/iai.65.12.5326-5329.1997 (1997).
73 Safley, S. A., Cluff, C. W., Marshall, N. E. & Ziegler, H. K. Role of listeriolysin-O (LLO) in the T lymphocyte response to infection with Listeria monocytogenes. Identification of T cell epitopes of LLO. *J Immunol* **146**, 3604-3616 (1991).

74 Laine, R. O., Zeile, W., Kang, F., Purich, D. L. & Southwick, F. S. Vinculin proteolysis unmasks an ActA homolog for actin-based Shigella motility. *J Cell Biol* **138**, 1255-1264, doi:10.1083/jcb.138.6.1255 (1997).

75 King, M. T., Huh, I., Shenai, A., Brooks, T. M. & Brooks, C. L. Structural basis of VHH-mediated neutralization of the food-borne pathogen Listeria monocytogenes. *J Biol Chem* **293**, 13626-13635, doi:10.1074/jbc.RA118.003888 (2018).

76 Calderon-Gonzalez, R. *et al.* Identification and characterisation of T-cell epitopes for incorporation into dendritic cell-delivered Listeria vaccines. *J Immunol Methods* **424**, 111-119, doi:10.1016/j.jim.2015.05.009 (2015).

77 Mendonca, M. *et al.* Fructose 1,6-Bisphosphate Aldolase, a Novel Immunogenic Surface Protein on Listeria Species. *PLoS One* **11**, e0160544, doi:10.1371/journal.pone.0160544 (2016).

78 Renier, S., Micheau, P., Talon, R., Hebraud, M. & Desvaux, M. Subcellular localization of extracytoplasmic proteins in monoderm bacteria: rational secretomics-based strategy for genomic and proteomic analyses. *PLoS One* **7**, e42982, doi:10.1371/journal.pone.0042982 (2012).

79 Bettencourt, P. *et al.* Identification of antigens presented by MHC for vaccines against tuberculosis. *NPJ Vaccines* **5**, 2, doi:10.1038/s41541-019-0148-y (2020).

80 Hess, J. *et al.* Superior efficacy of secreted over somatic antigen display in recombinant Salmonella vaccine induced protection against listeriosis. *Proc Natl Acad Sci U S A* **93**, 1458-1463, doi:10.1073/pnas.93.4.1458 (1996).

81 McMurtrey, C. *et al.* T cell recognition of Mycobacterium tuberculosis peptides presented by HLA-E derived from infected human cells. *PLoS One* **12**, e0188288, doi:10.1371/journal.pone.0188288 (2017).

82 Karunakaran, K. P. *et al.* Outer membrane proteins preferentially load MHC class II peptides: implications for a Chlamydia trachomatis T cell vaccine. *Vaccine* **33**, 2159-2166, doi:10.1016/j.vaccine.2015.02.055 (2015).

83 Jensen, L. J. *et al.* STRING 8--a global view on proteins and their functional interactions in 630 organisms. *Nucleic acids research* **37**, D412-416, doi:gkn760 [pii]

10.1093/nar/gkn760 (2009).

84 Dallo, S. F., Kannan, T. R., Blaylock, M. W. & Baseman, J. B. Elongation factor Tu and E1 beta subunit of pyruvate dehydrogenase complex act as fibronectin binding proteins in Mycoplasma pneumoniae. *Mol Microbiol* **46**, 1041-1051, doi:10.1046/j.1365-2958.2002.03207.x (2002).

85 Furano, A. V. Content of elongation factor Tu in Escherichia coli. *Proc Natl Acad Sci U S A* **72**, 4780-4784, doi:10.1073/pnas.72.12.4780 (1975).

86 Kopeckova, M., Pavkova, I. & Stulik, J. Diverse Localization and Protein Binding Abilities of Glyceraldehyde-3-Phosphate Dehydrogenase in Pathogenic Bacteria: The Key to its Multifunctionality? *Front Cell Infect Microbiol* **10**, 89, doi:10.3389/fcimb.2020.00089 (2020).

87 Bierne, H. & Cossart, P. Listeria monocytogenes surface proteins: from genome predictions to function. *Microbiology and molecular biology reviews : MMBR* **71**, 377-397, doi:10.1128/mmbr.00039-06 (2007).

88 Schuerch, D. W., Wilson-Kubalek, E. M. & Tweten, R. K. Molecular basis of listeriolysin O pH dependence. *Proc Natl Acad Sci U S A* **102**, 12537-12542, doi:10.1073/pnas.0500558102 (2005).

89 Koster, S. *et al.* Crystal structure of listeriolysin O reveals molecular details of oligomerization and pore formation. *Nat Commun* **5**, 3690, doi:10.1038/ncomms4690 (2014).

90 Xiang, Z. & He, Y. Genome-wide prediction of vaccine targets for human herpes simplex viruses using Vaxign reverse vaccinology. *BMC Bioinformatics* **14 Suppl 4**, S2, doi:10.1186/1471-2105-14-S4-S2 (2013).

91 Ong, E. *et al.* Vaxign2: the second generation of the first Web-based vaccine design program using reverse vaccinology and machine learning. *Nucleic Acids Res* **49**, W671-W678, doi:10.1093/nar/gkab279 (2021).

92 Ong, E. *et al.* Vaxign-ML: supervised machine learning reverse vaccinology model for improved prediction of bacterial protective antigens. *Bioinformatics* **36**, 3185-3191, doi:10.1093/bioinformatics/btaa119 (2020).

93 Verbeke, R. *et al.* Broadening the Message: A Nanovaccine Co-loaded with Messenger RNA and alpha-GalCer Induces Antitumor Immunity through Conventional and Natural Killer T Cells. *ACS Nano* **13**, 1655-1669, doi:10.1021/acsnano.8b07660 (2019).

94 Jiang, W. *et al.* A two-adjuvant multiantigen candidate vaccine induces superior protective immune responses against SARS-CoV-2 challenge. *Cell Rep* **37**, 110112, doi:10.1016/j.celrep.2021.110112 (2021).

95 Gabitzsch, E. *et al.* Dual-Antigen COVID-19 Vaccine Subcutaneous Prime Delivery With Oral Boosts Protects NHP Against SARS-CoV-2 Challenge. *Front Immunol* **12**, 729837, doi:10.3389/fimmu.2021.729837 (2021).

96 Giguere, S. *et al.* MHC-NP: predicting peptides naturally processed by the MHC. *J Immunol Methods* **400-401**, 30-36, doi:10.1016/j.jim.2013.10.003 (2013).

97 Lurie, N., Saville, M., Hatchett, R. & Halton, J. Developing Covid-19 Vaccines at Pandemic Speed. *N Engl J Med* **382**, 1969-1973, doi:10.1056/NEJMp2005630 (2020).

98 Chen, C. *et al.* The Listeriolysin O PEST-like Sequence Co-opts AP-2-Mediated Endocytosis to Prevent Plasma Membrane Damage during Listeria Infection. *Cell Host Microbe* **23**, 786-795 e785, doi:10.1016/j.chom.2018.05.006 (2018).

99 Michelet, C., Avril, J. L., Cartier, F. & Berche, P. Inhibition of intracellular growth of Listeria monocytogenes by antibiotics. *Antimicrob Agents Chemother* **38**, 438-446, doi:10.1128/AAC.38.3.438 (1994).

100 Suarez, M., Gonzalez-Zorn, B., Vega, Y., Chico-Calero, I. & Vazquez-Boland, J. A. A role for ActA in epithelial cell invasion by Listeria monocytogenes. *Cell Microbiol* **3**, 853-864, doi:10.1046/j.1462-5822.2001.00160.x (2001).

101 Cossart, P. & Sansonetti, P. J. Bacterial invasion: the paradigms of enteroinvasive pathogens. *Science* **304**, 242-248, doi:10.1126/science.1090124 (2004).

102 Gonzalez-Galarza, F. F. *et al.* Allele frequency net database (AFND) 2020 update: gold-standard data classification, open access genotype data and new query tools. *Nucleic Acids Res* **48**, D783-D788, doi:10.1093/nar/gkz1029 (2020).

103 Partridge, T. *et al.* Discrimination Between Human Leukocyte Antigen Class I-Bound and Co-Purified HIV-Derived Peptides in Immunopeptidomics Workflows. *Front Immunol* **9**, 912, doi:10.3389/fimmu.2018.00912 (2018).

104 Abelin, J. G. *et al.* MONTE enables serial immunopeptidome, ubiquitylome, proteome, phosphoproteome, acetylome analyses of sample-limited tissues. *bioRxiv* (2022).

105 Chong, C. *et al.* High-throughput and Sensitive Immunopeptidomics Platform Reveals Profound Interferongamma-Mediated Remodeling of the Human Leukocyte Antigen (HLA) Ligandome. *Mol Cell Proteomics* **17**, 533-548, doi:10.1074/mcp.TIR117.000383 (2018).

106 Nelde, A., Kowalewski, D. J. & Stevanovic, S. Purification and Identification of Naturally Presented MHC Class I and II Ligands. *Methods Mol Biol* **1988**, 123-136, doi:10.1007/978-1-4939-9450-2_10 (2019).

107 Borezee, E., Pellegrini, E. & Berche, P. OppA of Listeria monocytogenes, an oligopeptide-binding protein required for bacterial growth at low temperature and involved in intracellular survival. *Infect Immun* **68**, 7069-7077, doi:10.1128/IAI.68.12.7069-7077.2000 (2000).

108 Kanehisa, M. & Goto, S. KEGG: kyoto encyclopedia of genes and genomes. *Nucleic Acids Res* **28**, 27-30, doi:10.1093/nar/28.1.27 (2000).

109 Kanehisa, M. Toward understanding the origin and evolution of cellular organisms. *Protein Sci* **28**, 1947-1951, doi:10.1002/pro.3715 (2019).

110 Kanehisa, M., Furumichi, M., Sato, Y., Ishiguro-Watanabe, M. & Tanabe, M. KEGG: integrating viruses and cellular organisms. *Nucleic Acids Res* **49**, D545-D551, doi:10.1093/nar/gkaa970 (2021).

111 Toledo-Arana, A. *et al.* The Listeria transcriptional landscape from saprophytism to virulence. *Nature* **459**, 950-956, doi:10.1038/nature08080 (2009).

112 Gerlach, A. M. *et al.* Role of CD40 ligation in dendritic cell semimaturation. *BMC Immunol* **13**, 22, doi:10.1186/1471-2172-13-22 (2012).

113 Brennan, P. J., Brigl, M. & Brenner, M. B. Invariant natural killer T cells: an innate activation scheme linked to diverse effector functions. *Nat Rev Immunol* **13**, 101-117, doi:10.1038/nri3369 (2013).

114 Ranson, T. *et al.* Invariant V alpha 14+ NKT cells participate in the early response to enteric Listeria monocytogenes infection. *J Immunol* **175**, 1137-1144, doi:10.4049/jimmunol.175.2.1137 (2005).

115 Yu, Y. *et al.* Elongation Factor Thermo Unstable (EF-Tu) Moonlights as an Adhesin on the Surface of Mycoplasma hyopneumoniae by Binding to Fibronectin. *Front Microbiol* **9**, 974, doi:10.3389/fmicb.2018.00974 (2018).

116 Harvey, K. L., Jarocki, V. M., Charles, I. G. & Djordjevic, S. P. The Diverse Functional Roles of Elongation Factor Tu (EF-Tu) in Microbial Pathogenesis. *Front Microbiol* **10**, 2351, doi:10.3389/fmicb.2019.02351 (2019).

117 Carrasco, S. E. *et al.* Borrelia burgdorferi elongation factor EF-Tu is an immunogenic protein during Lyme borreliosis. *Emerg Microbes Infect* **4**, e54, doi:10.1038/emi.2015.54 (2015).

118 Sanchez-Campillo, M. *et al.* Identification of immunoreactive proteins of Chlamydia trachomatis by Western blot analysis of a two-dimensional electrophoresis map with patient sera. *Electrophoresis* **20**, 2269-2279, doi:10.1002/(SICI)1522-2683(19990801)20:11<2269::AID-ELPS2269>3.0.CO;2-D (1999).

119 Lock, R. A. *et al.* Proteome analysis of highly immunoreactive proteins of Helicobacter pylori. *Helicobacter* **7**, 175-182, doi:10.1046/j.1523-5378.2002.00078.x (2002).

120 Lathe, W. C., 3rd & Bork, P. Evolution of tuf genes: ancient duplication, differential loss and gene conversion. *FEBS Lett* **502**, 113-116, doi:10.1016/s0014-5793(01)02639-4 (2001).

121 Teran-Navarro, H. *et al.* A Comparison Between Recombinant Listeria GAPDH Proteins and GAPDH Encoding mRNA Conjugated to Lipids as Cross-Reactive Vaccines for Listeria, Mycobacterium, and Streptococcus. *Front Immunol* **12**, 632304, doi:10.3389/fimmu.2021.632304 (2021).

122 Sajid, A. *et al.* mRNA vaccination induces tick resistance and prevents transmission of the Lyme disease agent. *Sci Transl Med* **13**, eabj9827, doi:10.1126/scitranslmed.abj9827 (2021).

123 Schneider, C., Newman, R. A., Sutherland, D. R., Asser, U. & Greaves, M. F. A one-step purification of membrane proteins using a high efficiency immunomatrix. *J Biol Chem* **257**, 10766-10769 (1982).

124 Zhang, J. *et al.* PEAKS DB: de novo sequencing assisted database search for sensitive and accurate peptide identification. *Mol Cell Proteomics* **11**, M111 010587, doi:10.1074/mcp.M111.010587 (2012).

125 Martens, L., Vandekerckhove, J. & Gevaert, K. DBToolkit: processing protein databases for peptide-centric proteomics. *Bioinformatics (Oxford, England)* **21**, 3584-3585, doi:10.1093/bioinformatics/bti588 (2005).

126 Cox, J. & Mann, M. MaxQuant enables high peptide identification rates, individualized p.p.b.-range mass accuracies and proteome-wide protein quantification. *Nature biotechnology* **26**, 1367-1372, doi:10.1038/nbt.1511 (2008).

127 Tyanova, S. *et al.* The Perseus computational platform for comprehensive analysis of (prote)omics data. *Nature methods* **13**, 731-740, doi:10.1038/nmeth.3901 (2016).
128 Bittremieux, W. spectrum_utils: A Python Package for Mass Spectrometry Data Processing and Visualization. *Anal Chem* **92**, 659-661, doi:10.1021/acs.analchem.9b04884 (2020).
129 Levitsky, L. I., Klein, J. A., Ivanov, M. V. & Gorshkov, M. V. Pyteomics 4.0: Five Years of Development of a Python Proteomics Framework. *J Proteome Res* **18**, 709-714, doi:10.1021/acs.jproteome.8b00717 (2019).
130 Becavin, C. *et al.* Listeriomics: an Interactive Web Platform for Systems Biology of Listeria. *mSystems* **2**, doi:10.1128/mSystems.00186-16 (2017).
131 Leung, N., Gianfelice, A., Gray-Owen, S. D. & Ireton, K. Impact of the Listeria monocytogenes protein InlC on infection in mice. *Infect Immun* **81**, 1334-1340, doi:10.1128/IAI.01377-12 (2013).
132 Perez-Riverol, Y. *et al.* The PRIDE database and related tools and resources in 2019: improving support for quantification data. *Nucleic Acids Res* **47**, D442-D450, doi:10.1093/nar/gky1106 (2019).
133 Andreatta, M. & Nielsen, M. Gapped sequence alignment using artificial neural networks: application to the MHC class I system. *Bioinformatics* **32**, 511-517, doi:10.1093/bioinformatics/btv639 (2016).
134 Nielsen, M. *et al.* Reliable prediction of T-cell epitopes using neural networks with novel sequence representations. *Protein Sci* **12**, 1007-1017, doi:10.1110/ps.0239403 (2003).
135 Jurtz, V. *et al.* NetMHCpan-4.0: Improved Peptide-MHC Class I Interaction Predictions Integrating Eluted Ligand and Peptide Binding Affinity Data. *J Immunol* **199**, 3360-3368, doi:10.4049/jimmunol.1700893 (2017).
136 Nielsen, M. & Andreatta, M. NetMHCpan-3.0; improved prediction of binding to MHC class I molecules integrating information from multiple receptor and peptide length datasets. *Genome Med* **8**, 33, doi:10.1186/s13073-016-0288-x (2016).
137 Hoof, I. *et al.* NetMHCpan, a method for MHC class I binding prediction beyond humans. *Immunogenetics* **61**, 1-13, doi:10.1007/s00251-008-0341-z (2009).
138 Geginat, G., Schenk, S., Skoberne, M., Goebel, W. & Hof, H. A novel approach of direct ex vivo epitope mapping identifies dominant and subdominant CD4 and CD8 T cell epitopes from Listeria monocytogenes. *J Immunol* **166**, 1877-1884, doi:10.4049/jimmunol.166.3.1877 (2001).
139 Galperin, M. Y., Makarova, K. S., Wolf, Y. I. & Koonin, E. V. Expanded microbial genome coverage and improved protein family annotation in the COG database. *Nucleic Acids Res* **43**, D261-269, doi:10.1093/nar/gku1223 (2015).
140 Galperin, M. Y. *et al.* COG database update: focus on microbial diversity, model organisms, and widespread pathogens. *Nucleic Acids Res* **49**, D274-D281, doi:10.1093/nar/gkaa1018 (2021).

ACKNOWLEDGEMENTS

We are grateful to Prof. Pascale Cossart for sharing the *Listeria monocytogenes* EGD strain. We thank Jarne Pauwels and Jonas Erzeel for technical assistance and the VIB Proteomics Core for LC-MS/MS analysis. R.L.M. is supported by the Flemish Institute for Biotechnology (VIB) and a faculty interim fellowship from the UGent Faculty of Medicine and Health Sciences. R.V. is funded by a UGent BOF postdoc grant (BOF20/PDO/041) and A.G. is supported by a PhD fellowship from the Higher Education Commission (HEC) Pakistan. F.I. acknowledges support from Odysseus grant G0F8616N from the Research Foundation Flanders (FWO) and D.E. is funded by a FWO PhD fellowship for fundamental research. F.I., L.M., B.V. and I.L. acknowledge support from Ghent University Concerted Research Action grant BOF21/GOA/033.

AUTHOR CONTRIBUTIONS

R.M. performed the *in vitro Listeria* infection and immunopeptidomics experiments, compiled all figures and wrote and edited the paper. R.V. and I.A. performed mRNA transcription and production of mRNA Galsomes, assisted C.A. with vaccination and *Listeria* challenge assays, performed the vaccination and T-cell response measurements and wrote and edited the paper. K.B. cloned and prepared the plasmids for mRNA transcription. C.A. performed the vaccination and *Listeria* challenge assays, assisted R.V. and I.A. with the vaccination and T-cell response measurements and wrote and edited the paper. D.E. assisted R.V., I.A. and C.A. with vaccination, *Listeria* challenge and T-cell response experiments. A.G. performed *in vitro Listeria* infection and western blotting experiments to test MHC Class II expression, while I.A. performed read-out by flow cytometry. F.T. supervised A.G., generated figures and edited the paper. H.D. produced synthetic peptides for immunopeptide validation. T.M.M. assisted R.M. with immunopeptidomics data analysis and R.G. assisted with spectral validation of the synthetic immunopeptides. C.B. assisted R.M. with the conservation analysis of *Listeria* antigens and epitopes and edited the paper. L.M. supervised R.G. and edited the paper. S.D.S. supervised R.V. and I.A. and edited the paper. B.V. provided the W6/32 antibody for the immunopeptidomics experiments, assisted in data interpretation and edited the paper. I.L. supervised R.V. and I.A., assisted in data interpretation of the vaccination challenge and T-cell response measurements and wrote and edited the paper. F.I. conceptualized and initiated the project, supervised R.M, C.A., A.G, D.E., K.B. and F.T., interpreted the immunopeptidomics data, managed data compilation and data interpretation, generated figures, and wrote and edited the paper.

COMPETING INTERESTS

The authors declare the following competing interests: patent application no. EP22170845.6, Vaccine Compositions against Listeria infection.

FIGURE LEGENDS

Figure 1. Identification of MHC class I immunopeptides presented on *Listeria*-infected HeLa and HCT-116 cells. (A) Four replicates of *Listeria*-infected and uninfected HeLa or HCT-116 cells were dissolved using a mild lysis buffer and purified as described [61]. One half of the resulting immunopeptides was analyzed by label-free LC-MS/MS analysis on a Q Exactive HF mass spectrometer, while the other half was differentially labeled by TMT, pooled per cell line and fractionated into 12 fractions prior to LC-MS/MS analysis on a Fusion Lumos. Database searching was carried out using PEAKS Studio X [124,127]. **(B)** Overview of identified and quantified immunopeptides per cell line and in total. **(C)** Immunopeptide length distribution representing the typical dominance of 9mers in the human MHC I-presented immunopeptidome. **(D)** 9mer peptide sequences were submitted to MixMHCp 2.1 for motif deconvolution using sequence logos for visualization of the modelled position weight matrices (PWMs) after unsupervised clustering [64,65]. To this end, the tool assumes that all peptides are of length equal to core length, are naturally aligned and that defined positions at the beginning (first three amino acids) and end (last two positions) can be found in the peptide sequence, which is typically the case for HLA-I ligands. HLA binding motifs derived from experimental data demonstrated good overall matching with the expected cell line-specific NetMHCpan 4.1 reference motifs [66,133,134]. For HeLa cells, two out of three motifs could be fully restored, while the motif for HLA-C*12:03 was only partially recovered. For HCT-116, five out of six HLA motifs were fully reconstituted, while HLA-C*07:01 was only incompletely recovered, likely due to typically low expression levels of many HLA-C alleles [61]. **(E)** Principal component analysis (PCA) using the immunopeptide intensities separated the uninfected samples from the *Listeria*-infected samples.

Figure 2. Detection of high confident *Listeria* epitopes. (A) Filtering of *Listeria* peptides for detection in at least two infected samples, higher overall abundance in infected samples and absence in human proteins resulted 68 high confident bacterial epitopes from 42 *Listeria* protein antigens (Supplementary Table 2). **(B)** Peptide binding affinity prediction using the NetMHCpan EL 4.1 algorithm demonstrated that the large majority of the high confidence *Listeria* peptides are indeed predicted to bind to at least one HLA class I allele of the respective cell line [67,135-137]. **(C)** A selection of 24 *Listeria* immunopeptide sequences was synthesized to compare their synthetic and experimental fragmentation spectra, confirming the *bona fide* identification of the four epitopes shown here and in Supplementary Figure 3. The correlation coefficient r is shown for each *Listeria*-synthetic peptide pair (see materials and methods). **(D)** Volcano plots showing that the high confident *Listeria* immunopeptides belong to the most upregulated epitopes upon infection in both cellular models. **(E)** Likewise, heat maps visualizing individual *Listeria* peptide intensities (z-scored) following label-free quantitation show that peptides are generally absent in the uninfected control samples, while TMT-labeling data demonstrates more low-level background intensities presumably due to ratio suppression [68,69]. Epitopes identified by both label-free and TMT workflows are indicated by an asterisk (*),

including the previously described VAYGRQVYL epitope from LLO [138]. Two versions of each heat map are shown, with the left one indicating z-scored intensities after imputing empty values with low values around the detection limit (to allow t-testing). The heat maps on the right are identical, but show originally missing (unimputed) values in grey. **(F)** Venn diagrams showing the overlap between both cell lines in presented *Listeria* epitopes (top) and their parent protein antigens (bottom). Only a single epitope (HLVPEFTNEV) was detected on both cell lines, while the overlap at the antigen level is substantially higher with seven *Listeria* proteins being presented by the two cellular models.

Figure 3. *Listeria* antigens are often derived from the bacterial periphery. (A) Subcellular localization prediction of *Listeria* antigens indicated that the majority of antigens are localized at the bacterial periphery as either cell surface-associated or extracellular proteins [78]. **(B)** Clusters of Orthologous Groups (COG) terms assessment corroborated the importance of cell wall and membrane-associated proteins for presentation as antigens [139,140] **(C)** Histogram showing the number of identified epitopes for all 42 detected *Listeria* antigens. The seven most presented antigens without any known enzymatic or harmful activity to host cells were selected as vaccination targets (green bars). Antigens with multiple epitopes identified but known enzymatic or toxic properties were excluded from further assessment as vaccine candidates (red bars). Most of these selected antigens were identified from both cell types and are predicted to be present at the bacterial surface. **(D)** Vaxign-ML scores were calculated for all 2,847 *Listeria monocytogenes* EGD proteins and plotted according to scoring rank [91]. The seven selected *Listeria* antigens were among the top scoring proteins, further supporting their selection as vaccine candidate. **(E)** Box plot showing the Vaxign-ML scores for all 2,847 EGD proteins, the 42 identified *Listeria* antigens and the seven selected antigens. The latter showed the highest average score, followed by all identified *Listeria* antigens, both scoring significantly higher than the average score of all EGD proteins (Mann-Whitney non-parametrical testing, * p-value <0.05, **** p-value < 0.0001).

Figure 4. Highly presented antigens provide protection as mRNA vaccine candidates. (A) C57BL6 mice were vaccinated with a prime-boost regime utilizing full length, mRNA-encoded *Listeria* antigens formulated as lipid nano vesicles including α-GC as adjuvant. All seven selected antigen candidates were each tested in one independent experiment (experiments 1 and 2), each time containing 5 mice/group. Additional experiments for lmon_0149 and LLO_E262K are shown in Supplementary Figure 5 (experiments 3 and 4). In both experiments 1 and 2, mice were vaccinated by tail vein injection of the prime vaccine comprising 10 µg of the indicated *Listeria* antigen mRNA. As negative control and inter-experiment reference, 10 µg ovalbumin (OVA) mRNA was injected in both experiments. In the first experiment, we also administered a combination vaccine containing 5 µg LLO_E262K mRNA mixed with 5 µg mRNA of OppA lmon_2272. In the second experiment, injection of PBS was included as additional negative control, while a low-dose infection with *Listeria monocytogenes* EGD ($1x10^4$ CFUs) was included

as positive control for successful immunization. Two weeks after prime vaccination, an identical booster was administered and two weeks later the animals were challenged by intravenous injection of $7.5x10^5$ bacteria. Mice were euthanized 72 hours post-challenge and the bacterial load in spleen and liver was assessed by counting colony-forming units (CFU) after serial dilution and replating. **(B)** Bar charts depicting the number of CFUs in spleen (upper) and liver (lower) relative to the OVA negative control on a log scale. All *Listeria* vaccines reduced the bacterial burden in spleen and liver, while only OppA lmon_0149, EF-Tu and the combination vaccine reached statistical significance in both organs (Mann-Whitney test, * p value <0.05 ** p value <0.01). (**C-D**) Pearson (C) and Spearman rank (D) correlation analysis using GraphPad Prism 9.3 was carried out between the number of identified bacterial epitopes per vaccine candidate and vaccination efficacy expressed as % CFU reduction. For the combination vaccine, the number of epitopes for both antigens was summed up. In both liver and spleen, a positive correlation between the number of presented epitopes and protective efficacy is indicated by positive r values, although without reaching statistical significance. Data points in (C) were fitted with a non-linear hyperbolic function.

Figure 5. Specific CD8+ T-cell responses upon lmon_0149 vaccination. C57BL/6J mice were vaccinated with mRNA galsomes encoding lmon_0149 **(A)** or OVA as control **(B)** (10 mice/group). After 7 days, splenocytes were isolated and pulsed with a control OVA epitope or two synthetic peptide epitopes predicted from the lmon_0149 sequence using the IEDB resource tools NetMHCpan [67] and MHC-NP [96]. **(A)** Mice vaccinated with lmon_0149 showed significantly higher levels of CD8+ T-cells responses to both lmon_0149 YSYKFIRV and QVFEGLYTL epitopes as compared to the OVA epitope SIINFEKL (Shapiro-Wilk test confirmed data normality, paired t test applied, ** p value <0.01 **** p value <0.0001, 3 data points with <35% cell viability were excluded). **(B)** Conversely, OVA-vaccinated mice responded well to SIINFEKL but not to YSYKFIRV, confirming that mRNA vaccination with lmon_0149 elicits specific CD8+ T-cell responses against this *Listeria* antigen (Shapiro-Wilk test rejected data normality, Wilcoxon matched-pairs signed rank test applied, ** p value <0.01). Additional control experiments with OVA-vaccinated or PBS-injected mice are shown in Supplementary Figure 6.

Supplementary Figure 1. HeLa cells do not express MHC-II during *Listeria* infection. (A-B) HeLa cells or JY cells (B cell line) were either infected with *Listeria monocytogenes* EGD (*Listeria*) for 24 h at MOI 25, or treated with 10 ng/mL interferon-γ for 48 h or left untreated. After infection, cells were either processed for western-blot (A) or flow cytometry (B) analysis. (A) MHC-I (anti-HLA-ABC) and MHC-II (anti-HLA-DM and -DR) were monitored by western blotting. Immunoblots against tubulin, listeriolysin O (LLO) and STAT1 serve as controls for loading, *Listeria* infection and interferon-γ treatment, respectively. (B) MHC-II (top panels) and MHC-I (bottom panels) were monitored by flow cytometry to determine their abundance on the cell surface in untreated, *Listeria* infected and interferon-γ-treated cells. Intensity signals

for MHC-II and -I molecules are shown relative to unstained cells. **(C)** Work flow describing the flow cytometry gating strategy used in (B). From left to right, exclusion of cell debris was performed by gating FSC-A versus SSC-A. This was followed by removal of cell aggregates by gating according to FSC-H/FSC-A parameters. Next, the removal of cell aggregates was performed by gating according to SSC-H/SSC-A parameters. Finally, dead cells were excluded from analysis by gating using Zombie green versus SSC-A parameter. Selected cells were analyzed to determine the abundance of MHC-II and –I molecule on cell surface.

Supplementary Figure 2. Listeria-derived immunopeptides preferentially bind to HLA-A alleles (A-B) For each 8-14mer immunopeptide, the HLA allele with the best % binding rank was determined using NetMHCpan 4.1 binding prediction (https://services.healthtech.dtu.dk/service.php?NetMHCpan-4.1). Interestingly, on both HeLa **(A)** and HCT-116 **(B)** cells the majority of immunopeptides showed the highest binding affinity for HLA-A alleles. This trend was even more pronounced for *Listeria*-derived epitopes of which ~80% showed strongest binding to HLA-A alleles in both HeLa and HCT-116 cells. Consequently, comparably fewer *Listeria* peptides showed high affinity for HLA-B and -C alleles. This could hint towards a favored presentation of bacterial peptides via HLA-A molecules, but further careful evaluation employing other pathogens and cell lines will be crucial to verify this hypothesis.

Supplementary Figure 3. Spectral comparison of *Listeria*-derived epitopes and their synthetic peptide counterpart. In order to verify the identified *Listeria*-derived immunopeptide sequences, a selection of 24 peptides were synthesized and recorded under the same LC-MS/MS conditions as the infection-derived samples. For TMT-derived sequences, synthetic peptides were also TMT labeled prior to analysis. Fragmentation spectra per sequence were compared by plotting positive relative abundance values for *Listeria*-derived and negative relative abundances for synthetic peptides. Fragment ions assigned to the *Listeria*-derived immunopeptide sequences by PEAKS Studio that matched with fragment ions in the spectra of the corresponding synthetic peptide were highlighted. The high degree of overlap between synthetic and *Listeria*-derived fragmentation spectra corroborates sequence identity, further indicated by high Pearson correlations ($r \geq 0.90$) calculated for all peptides and indicated for all spectral comparisons (see methods).

Supplementary Figure 4. STRING functional protein association. All 42 antigens of origin for the identified high confidence *Listeria* immunopeptides were subjected to the STRING database using their respective Lm EGDe homologs as input (due to Lm EGD not being available on STRING). Settings were kept at default (full STRING network, evidence based network edges, all interaction source to active, medium confidence (0.400) as minimum required interaction score, no interactors shown), and MCL clustering (inflation parameter 3.5) was selected as clustering method resulting in the annotation of nine

clusters. Connections between clusters are visualized with dotted lines. Proteins chosen as vaccine candidates are depicted with green squares. Cluster 1 includes three proteins localized at the cell surface associated with defense/virulence mechanism and cell wall/membrane biogenesis. Connected to cluster 1, cluster 2 consists of eight proteins of which most are included in the pVGC with plcA, LLO, mpl, actA and plcB, also including inlB, inlC and mntA. Localized in the extracellular milieu or on the cell surface, these proteins are involved in defense/virulence mechanism and cell wall/membrane biogenesis, but also associated with cell motility and amino acid transport and metabolism. The two proteins of cluster 3 show the same subcellular localization and are also involved in cell wall/membrane biogenesis, but are furthermore associated with the COG term posttranslational modification, protein turnover, chaperones. Proteins from cluster 4 localize to the extracellular milieu, cell surface and cytoplasm and are involved in cell cycle control, mitosis and meiosis as well as cell wall/membrane biogenesis. Cluster 5, which is not connected to any other cluster, includes three OppA proteins involved in amino acid transport and metabolism localizing to the extracellular milieu. Cluster 6 interconnecting cluster 3, 7 and 9, consists of four proteins localized at the cell surface involved in posttranslational modification, protein turnover, chaperones as well as energy production and conversion and also carbohydrate transport and metabolism. Both proteins of cluster 7, gap and fbaA, participate in carbohydrate transport and metabolism and are localized in the cytoplasm (like all proteins for cluster 8 and 9 also). Cluster 8 encompasses four proteins that contribute to energy production and conversion as well as amino acid transport and metabolism. The six protein members of cluster 9 finally are involved in transcription as well as translation and also replication, recombination and repair.

Supplementary Figure 5. Highly presented antigens provide protection as mRNA vaccine candidates. Next to the vaccination challenge experiments 1 and 2 shown in Figure 4, two additional independent experiments were performed using identical vaccine formulations for lmon_0149 and LLO_E262K (experiments 3 and 4). Experiment 4 further contained a vaccine formulation combining lmon_0149 and LLO_E262K. **(A-B)** Alternative visualization of the bar charts shown in Figure 4B, plotting non-normalized, absolute CFU values in log scale for experiments 1 and 2. **(C-D)** Bar charts depicting the non-normalized, absolute CFU counts measured for (C) lmon_0149 in experiments 2, 3 and 4 and for (D) LLO_E262K in experiments 1 and 4. Lmon_0149 vaccination showed consistently high levels of protection in spleen (~3 log CFU reduction) and liver (~1.5 to 2.5 log CFU reduction). In contrast, protection by LLO_E262K was not significant in most cases with lower CFU reductions of ~1.5 logs in spleen and liver. **(E)** Combining lmon_0149 and LLO_E262K in a single vaccine formulation did not yield additional or synergistic protective effects, confirming the rather low protection of LLO_E262K in our vaccination platform.

Supplementary Figure 6. Control T cell response measurements and flow cytometry gating strategy. **(A-B)** In an additional control experiment to the data shown in Figure 5, C57BL/6J mice were (A) vaccinated with mRNA galsomes encoding OVA or (B) injected with PBS (10 mice/group). After 7 days, splenocytes were isolated and pulsed with the OVA epitope SIINFEKL or the two lmon_0149 epitopes YSYKFIRV and QVFEGLYTL. No noticeable levels of IFN-γ^+ CD8 T cells could be detected upon pulsing with the lmon_0149 epitopes (average % IFN-γ^+ CD8 T cells < 0.14), while pulsing with the OVA-specific SIINFEKL peptide triggered statistically significant levels of IFN-γ^+ CD8 T cells in OVA-vaccinated mice (Shapiro-Wilk test rejected data normality, Wilcoxon matched-pairs signed rank test applied, ** p value <0.01, 2 data points with <35% cell viability were excluded). These results further support the specificity of the responses measured for the lmon_0149 epitopes shown in Figure 5. **(B)** Gating strategy employed for the data shown in (A). Panels from left to right show i) exclusion of debris from cells by gating FSC-A versus SSC-A, ii) removal of cell aggregates by gating according to FSC-H/FSC-A parameters and iii) by gating according to SSC-H/SSC-A parameters, iv) exclusion of dead cells by gating only for live/dead aqua-low cells, v) gate used to identify CD3e CD8a double positive cells, vi) antigen-reactive CD8a cells were defined as IFN-□+ expressing cells after peptide stimulation, and their frequencies were determined among total CD8a cells. The figure shows representative flow data of OVA vaccinated C57BL/6 mouse after pulsing with the QVFEGLYTL synthetic peptide. **(C)** Gating strategy used for the data presented in Figure 5. Panels from left to right show i) exclusion of debris from cells by gating FSC-A versus SSC-A, (ii) removal of cell aggregates by gating according to FSC-H/FSC-A parameters, iii) exclusion of dead cells by gating only for live/dead aqua-low cells, iv) gate used to identify CD8a positive cells, v) antigen-reactive CD8a cells were defined as IFN-□+ expressing cells after peptide stimulation, and their frequencies were determined among total CD8a cells. The figure shows representative flow data of lmon_0149 vaccinated C57BL/6 mouse after pulsing with the QVFEGLYTL synthetic peptide.

Supplementary Figure 7. Identified *Listeria* epitopes and antigens are well conserved. 264 fully sequenced *Listeria monocytogenes* strains were downloaded from NCBI RefSeq and used to create a BlastP database (Altschul et al. 1990) with all proteins annotated in these genomes. **(A)** We then ran BlastP (blast+ version 2.10 (Camacho et al. 2009) probing all 68 epitope peptide sequences identified from our experiments with *Listeria monocytogenes* EGD versus all the proteins of each genome. BlastP parameters were deliberately set non-stringent (evalue 1000, max_target_seqs 1) to retrieve only perfect matches with mapping identity equal to 100%. For each epitope we then plotted the percentage of strains in which the epitope sequence is fully conserved. Interestingly, the large majority (50 or 73%) of our identified epitopes were fully conserved in more than 95% of the strains, while another 13 epitopes (19%) were fully conserved in at least 50% of the strains. Only five epitopes were conserved in less than 50% of the investigated strains, indicating overall high conservation of the presented *Listeria* immunopeptides. **(B)**

Denotes the median antigen sequence similarity among all 264 *Listeria monocytogenes* strains indicating greater than 90% sequence similarity for all but two antigens. Antigens used in the mouse vaccination assays are depicted in green and show excellent sequence conservation of >95% in all strains. We therefore conclude that the chosen vaccine candidates will also hold substantial relevance not only for *Listeria monocytogenes* EGD, but also for more clinically relevant *Listeria* strains.

Figure 1

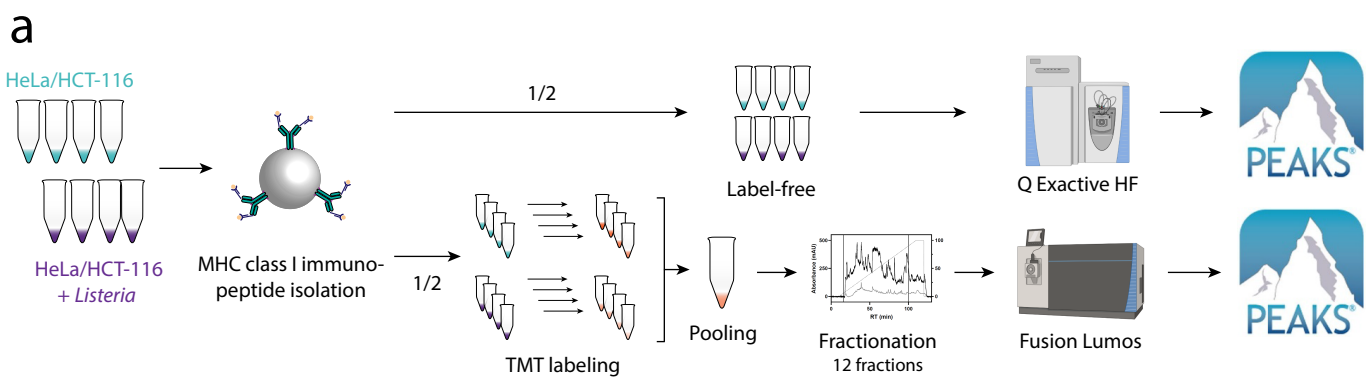
a
HeLa/HCT-116
HeLa/HCT-116
+ Listeria
MHC class I immuno-
peptide isolation
1/2
1/2
Label-free
Q Exactive HF
PEAKS
TMT labeling
Pooling
Fractionation
12 fractions
Fusion Lumos
PEAKS

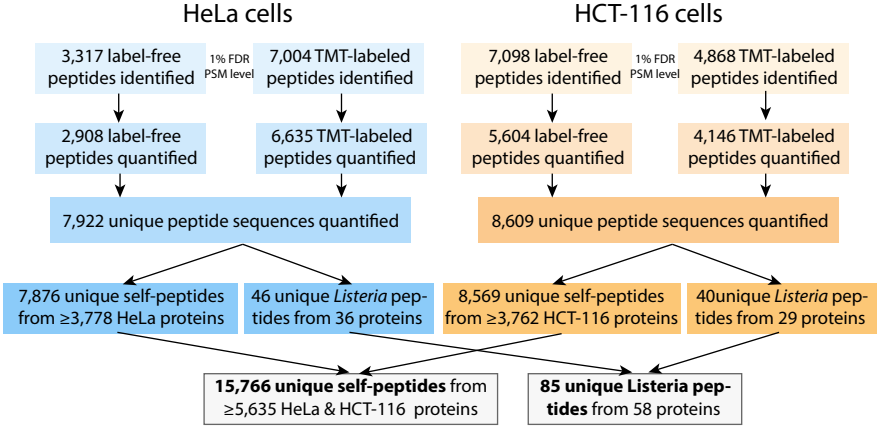
b
HeLa cells
HCT-116 cells
3,317 label-free peptides identified
1% FDR PSM level
7,004 TMT-labeled peptides identified
2,908 label-free peptides quantified
6,635 TMT-labeled peptides quantified
7,922 unique peptide sequences quantified
7,098 label-free peptides identified
1% FDR PSM level
4,868 TMT-labeled peptides identified
5,604 label-free peptides quantified
4,146 TMT-labeled peptides quantified
8,609 unique peptide sequences quantified
7,876 unique self-peptides from ≥3,778 HeLa proteins
46 unique Listeria peptides from 36 proteins
8,569 unique self-peptides from ≥3,762 HCT-116 proteins
40unique Listeria peptides from 29 proteins
15,766 unique self-peptides from ≥5,635 HeLa & HCT-116 proteins
85 unique Listeria peptides from 58 proteins

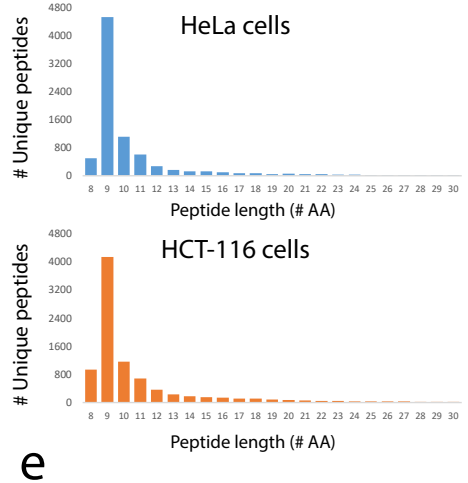
c
HeLa cells
Unique peptides
Peptide length (# AA)
HCT-116 cells
Unique peptides
Peptide length (# AA)

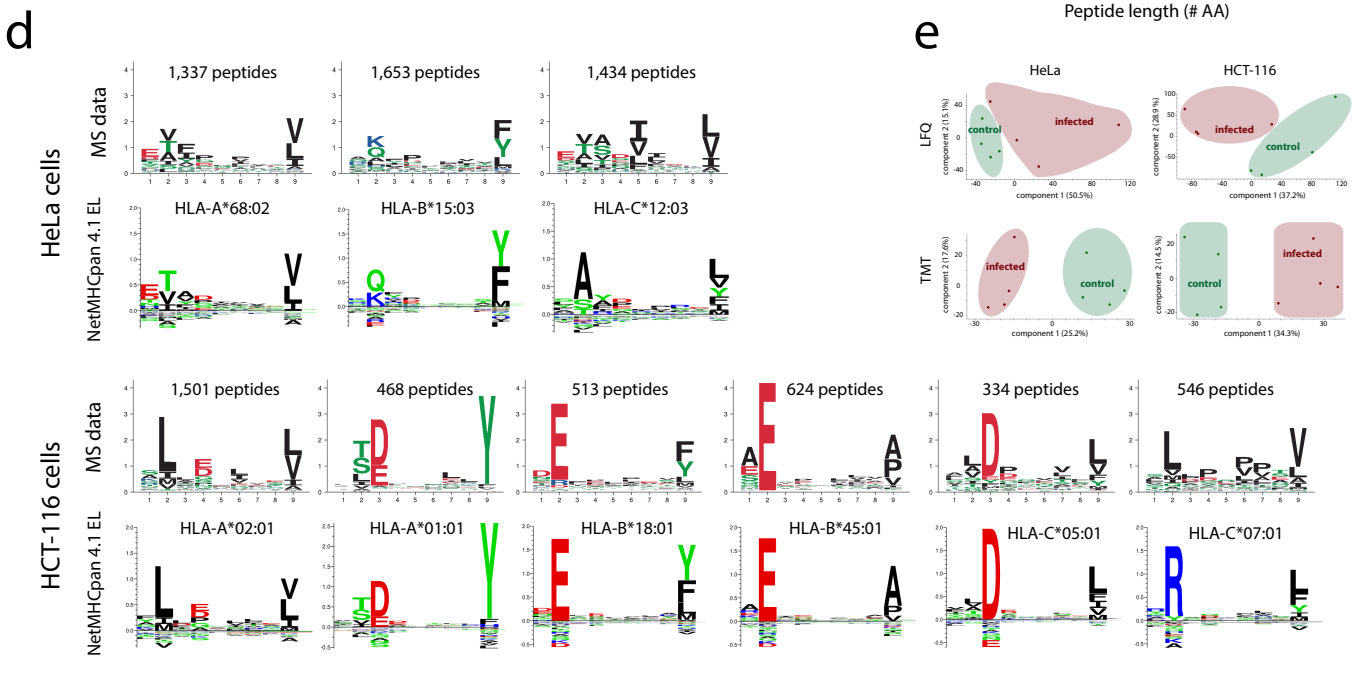
d
HeLa cells
MS data
1,337 peptides
1,653 peptides
1,434 peptides
NetMHCpan 4.1 EL
HLA-A*68:02
HLA-B*15:03
HLA-C*12:03
HCT-116 cells
MS data
1,501 peptides
468 peptides
513 peptides
624 peptides
334 peptides
546 peptides
NetMHCpan 4.1 EL
HLA-A*02:01
HLA-A*01:01
HLA-B*18:01
HLA-B*45:01
HLA-C*05:01
HLA-C*07:01

e
HeLa
HCT-116
LFQ
control
infected
component 1 (50.5%)
component 1 (37.2%)
TMT
component 1 (25.2%)
component 1 (34.3%)

Figure 2

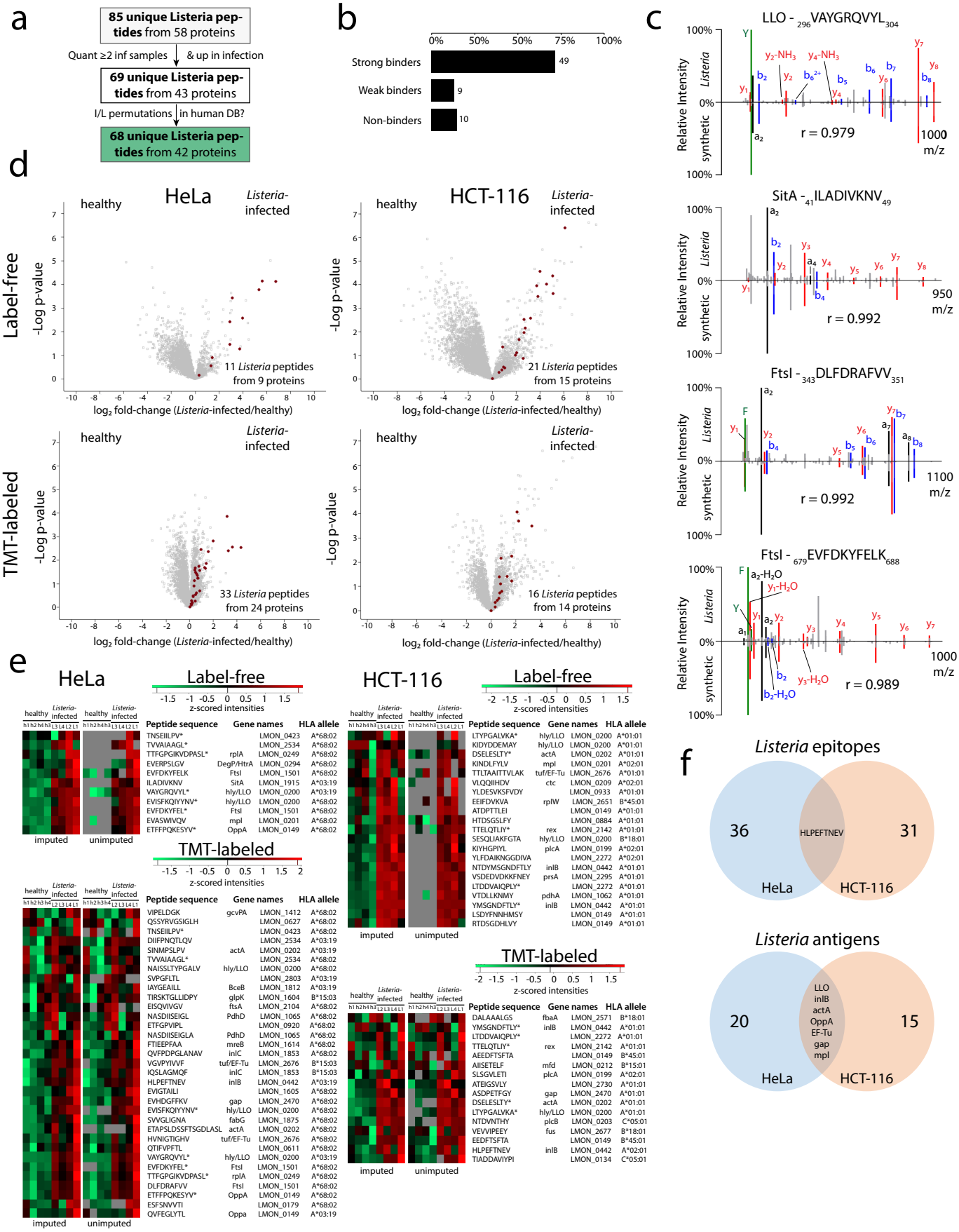
a
85 unique Listeria peptides from 58 proteins
Quant ≥2 inf samples
& up in infection
69 unique Listeria peptides from 43 proteins
I/L permutations
in human DB?
68 unique Listeria peptides from 42 proteins
b
0%
50%
50%
75%
100%
Strong binders
49
Weak binders
9
Non-binders
10
c
LLO - 296VAYGRQVYL304
SitA - 41ILADIVKNV49
FtsI - 343DLFDRAFVV351
FtsI - 679EVFDKYFELK688
Relative Intensity
Listeria
synthetic
100%
0%
r = 0.979
r = 0.992
r = 0.992
r = 0.989
1000 m/z
950 m/z
1100 m/z
d
Label-free
TMT-labeled
HeLa
HCT-116
healthy
Listeria-infected
-Log p-value
log2 fold-change (Listeria-infected/healthy)
11 Listeria peptides from 9 proteins
21 Listeria peptides from 15 proteins
33 Listeria peptides from 24 proteins
16 Listeria peptides from 14 proteins
e
HeLa
HCT-116
Label-free
TMT-labeled
z-scored intensities
imputed
unimputed
Peptide sequence
Gene names
HLA allele
TNSEIILPV*
LMON_0423
A*68:02
TVVAIAAGL*
LMON_2534
A*68:02
TTFGPGIKVDPASL*
rplA
LMON_0249
A*68:02
EVERPSLGV
DegP/HtrA
LMON_0294
A*68:02
EVFDKYFELK
FtsI
LMON_1501
A*68:02
ILADIVKNV
SitA
LMON_1915
A*03:19
VAYGRQVYL*
hly/LLO
LMON_0200
A*03:19
EVISFKQIYYNV*
hly/LLO
LMON_0200
A*68:02
EVFDKYFEL*
FtsI
LMON_1501
A*68:02
EVASWIVQV
mpl
LMON_0201
A*68:02
ETFFPQKESYV*
OppA
LMON_0149
A*68:02
VIPELDGK
gcvPA
LMON_1412
A*68:02
QSSYRVGSIGLH
LMON_0627
A*68:02
TNSEIILPV*
LMON_0423
A*68:02
DIIFPNQTLQV
LMON_2534
A*03:19
SINMPSLPV
actA
LMON_0202
A*03:19
TVVAIAAGL*
LMON_2534
A*68:02
NAISSLTYPGALV
hly/LLO
LMON_0200
A*68:02
SVPGFLTL
LMON_2803
A*03:19
IAYGEAILL
BceB
LMON_1812
A*03:19
TIRSKTGLLIDPY
glpK
LMON_1604
B*15:03
EISQVIVGV
ftsA
LMON_2104
A*68:02
NASDIISEIGL
PdhD
LMON_1065
A*68:02
ETFGPVIPL
LMON_0920
A*68:02
NASDIISEIGLA
PdhD
LMON_1065
A*68:02
FTIEEPFAA
mreB
LMON_1614
A*68:02
QVFPDPGLANAV
inlC
LMON_1853
A*68:02
VGVPYIVVF
tuf/EF-Tu
LMON_2676
B*15:03
IQSLAGMQF
inlC
LMON_1853
B*15:03
HLPEFTNEV
inlB
LMON_0442
A*03:19
EVIGTAILI
LMON_1605
A*68:02
EVHDGFFKV
gap
LMON_2470
A*68:02
EVISFKQIYYNV*
hly/LLO
LMON_0200
A*68:02
SVVGLIGNA
fabG
LMON_1875
A*68:02
ETAPSLDSSFTSGDLASL
actA
LMON_0202
A*68:02
HVNIGTIGHV
tuf/EF-Tu
LMON_2676
A*68:02
QTIFVPFTL
LMON_0611
A*68:02
VAYGRQVYL*
hly/LLO
LMON_0200
A*03:19
EVFDKYFEL*
FtsI
LMON_1501
A*68:02
TTFGPGIKVDPASL*
rplA
LMON_0249
A*68:02
DLFDRAFVV
FtsI
LMON_1501
A*68:02
ETFFPQKESYV*
OppA
LMON_0149
A*68:02
ESFSNVVTI
LMON_0179
A*68:02
QVFEGLYTL
Oppa
LMON_0149
A*03:19
LTYPGALVKA*
hly/LLO
LMON_0200
A*01:01
KIDYDDEMAY
hly/LLO
LMON_0200
A*01:01
DSELESLTY*
actA
LMON_0202
A*01:01
KINDLFYLV
mpl
LMON_0201
A*02:01
TTLTAAITTVLAK
tuf/EF-Tu
LMON_2676
A*01:01
VLQQIIHDV
ctc
LMON_0209
A*02:01
YLDESVKSFVDY
LMON_0933
A*01:01
EEIFDVKVA
rplW
LMON_2651
B*45:01
ATDPTTLEI
LMON_0149
A*01:01
HTDSGSLFY
LMON_0884
A*01:01
TTELQTLIY*
rex
LMON_2142
A*01:01
SESQLIAKFGTA
hly/LLO
LMON_0200
B*18:01
KIYHGPIYL
plcA
LMON_0199
A*02:01
YLFDAIKNGGDIVA
LMON_2272
A*02:01
NTDYMSGNDFTLY
inlB
LMON_0442
A*01:01
VSDEDVDKKFNEY
prsA
LMON_2295
A*01:01
LTDDVAIQPLY*
LMON_2272
A*01:01
VTDLLKNMY
pdhA
LMON_1062
A*01:01
YMSGNDFTLY*
inlB
LMON_0442
A*01:01
LSDYFNNHMSY
LMON_0149
A*01:01
RTDSGDHLVY
LMON_0149
A*01:01
DALAAALGS
fbaA
LMON_2571
B*18:01
YMSGNDFTLY*
inlB
LMON_0442
A*01:01
LTDDVAIQPLY*
LMON_2272
A*01:01
TTELQTLIY*
rex
LMON_2142
A*01:01
AEEDFTSFTA
LMON_0149
B*45:01
AIISETELF
mfd
LMON_0212
B*15:01
SLSGVLETI
plcA
LMON_0199
A*02:01
ATEIGSVLY
LMON_2730
A*01:01
ASDPETFGY
gap
LMON_2470
A*01:01
DSELESLTY*
actA
LMON_0202
A*01:01
LTYPGALVKA*
hly/LLO
LMON_0200
A*01:01
NTDVNTHY
plcB
LMON_0203
C*05:01
VEVVIPEEY
fus
LMON_2677
B*18:01
EEDFTSFTA
LMON_0149
B*45:01
HLPEFTNEV
inlB
LMON_0442
A*02:01
TIADDAVIYPI
LMON_0134
C*05:01
f
Listeria epitopes
36
HLPEFTNEV
31
HeLa
HCT-116
Listeria antigens
20
LLO
inlB
actA
OppA
EF-Tu
gap
mpl
15
HeLa
HCT-116

Figure 3

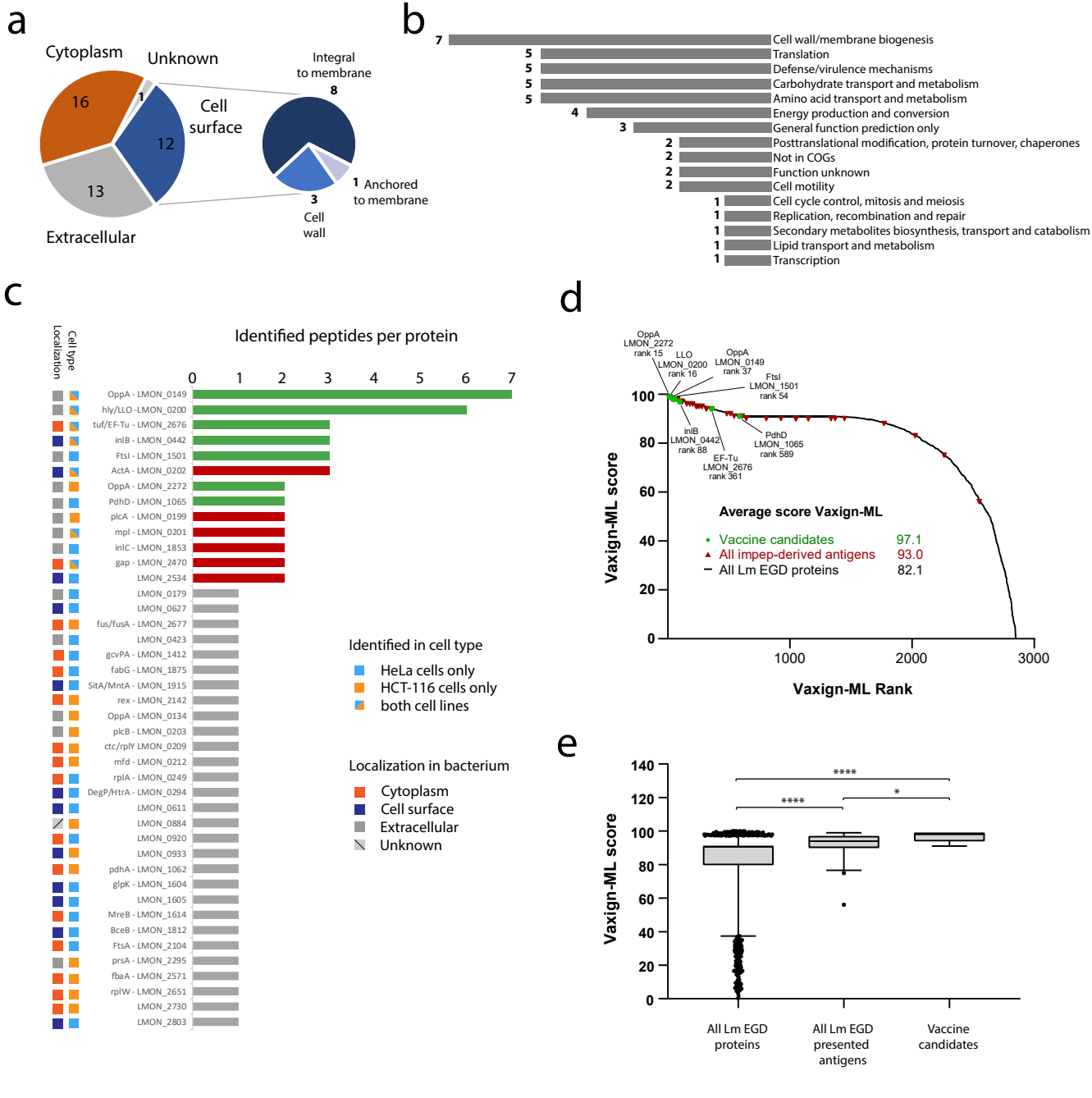
a
Cytoplasm
Unknown
Integral to membrane
16
1
8
Cell surface
12
13
1 Anchored to membrane
3
Cell wall
Extracellular
b
7 Cell wall/membrane biogenesis
5 Translation
5 Defense/virulence mechanisms
5 Carbohydrate transport and metabolism
5 Amino acid transport and metabolism
4 Energy production and conversion
3 General function prediction only
2 Posttranslational modification, protein turnover, chaperones
2 Not in COGs
2 Function unknown
2 Cell motility
1 Cell cycle control, mitosis and meiosis
1 Replication, recombination and repair
1 Secondary metabolites biosynthesis, transport and catabolism
1 Lipid transport and metabolism
1 Transcription
c
Localization
Cell type
Identified peptides per protein
0 1 2 3 4 5 6 7
OppA - LMON_0149
hly/LLO - LMON_0200
tuf/EF-Tu - LMON_2676
inlB - LMON_0442
FtsI - LMON_1501
ActA - LMON_0202
OppA - LMON_2272
PdhD - LMON_1065
plcA - LMON_0199
mpl - LMON_0201
inlC - LMON_1853
gap - LMON_2470
LMON_2534
LMON_0179
LMON_0627
fus/fusA - LMON_2677
LMON_0423
gcvPA - LMON_1412
fabG - LMON_1875
SitA/MntA - LMON_1915
rex - LMON_2142
OppA - LMON_0134
plcB - LMON_0203
ctc/rplY LMON_0209
mfd - LMON_0212
rplA - LMON_0249
DegP/HtrA - LMON_0294
LMON_0611
LMON_0884
LMON_0920
LMON_0933
pdhA - LMON_1062
glpK - LMON_1604
LMON_1605
MreB - LMON_1614
BceB - LMON_1812
FtsA - LMON_2104
prsA - LMON_2295
fbaA - LMON_2571
rplW - LMON_2651
LMON_2730
LMON_2803
Identified in cell type
HeLa cells only
HCT-116 cells only
both cell lines
Localization in bacterium
Cytoplasm
Cell surface
Extracellular
Unknown
d
OppA LMON_2272 rank 15
LLO LMON_0200 rank 16
OppA LMON_0149 rank 37
FtsI LMON_1501 rank 54
inlB LMON_0442 rank 88
EF-Tu LMON_2676 rank 361
PdhD LMON_1065 rank 589
Vaxign-ML score
Average score Vaxign-ML
Vaccine candidates 97.1
All impep-derived antigens 93.0
All Lm EGD proteins 82.1
Vaxign-ML Rank
e
Vaxign-ML score
****
****
*
All Lm EGD proteins
All Lm EGD presented antigens
Vaccine candidates

Figure 4

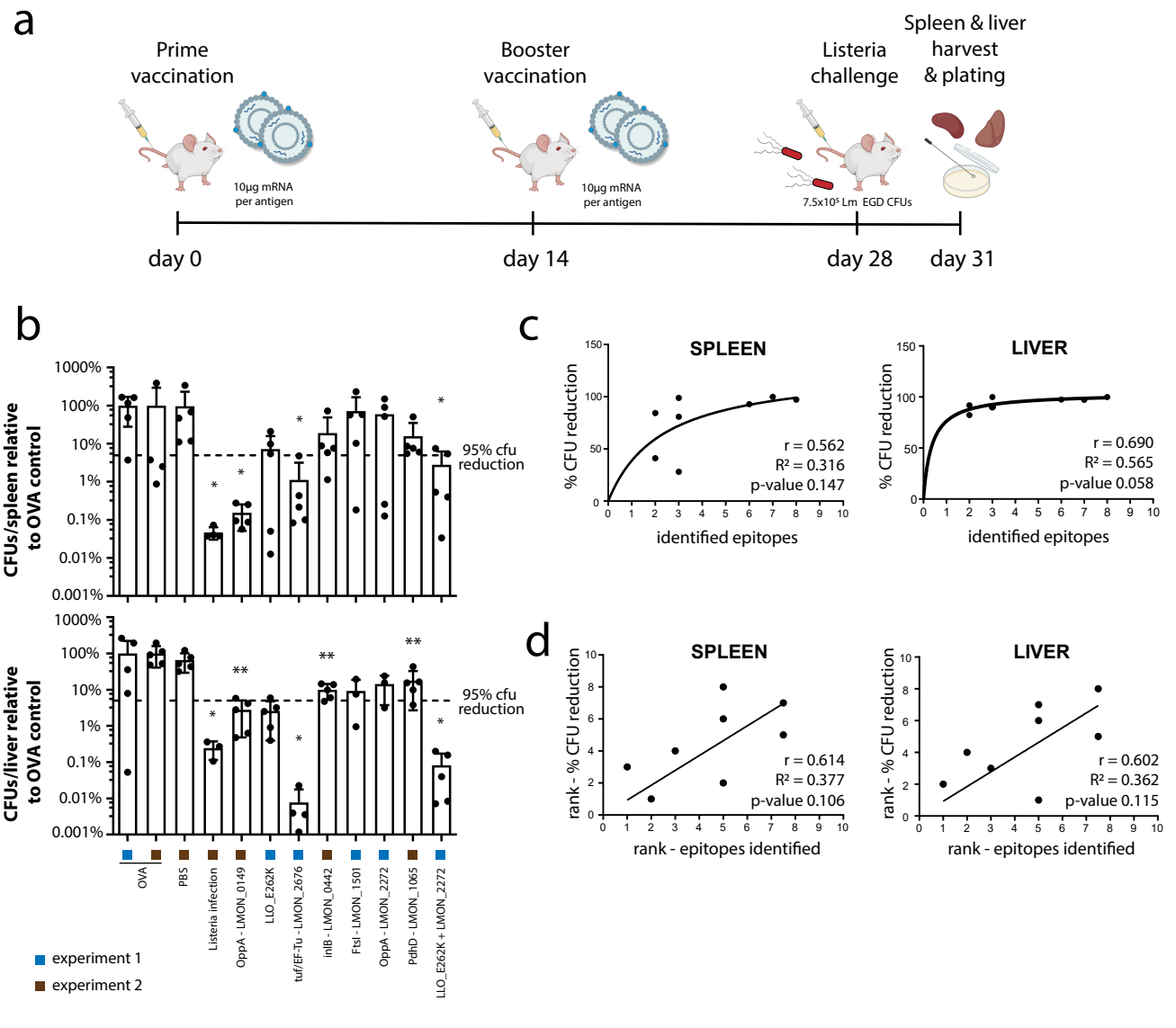
a
Prime vaccination
Booster vaccination
Listeria challenge
Spleen & liver harvest & plating
10µg mRNA per antigen
10µg mRNA per antigen
7.5x10⁵ Lm EGD CFUs
day 0
day 14
day 28
day 31
b
CFUs/spleen relative to OVA control
CFUs/liver relative to OVA control
1000%
100%
10%
1%
0.1%
0.01%
0.001%
95% cfu reduction
OVA
PBS
Listeria infection
OppA - LMON_0149
LLO_E262K
tuf/EF-Tu - LMON_2676
inlB - LMON_0442
FtsI - LMON_1501
OppA - LMON_2272
PdhD - LMON_1065
LLO_E262K + LMON_2272
experiment 1
experiment 2
c
SPLEEN
LIVER
% CFU reduction
identified epitopes
r = 0.562
R² = 0.316
p-value 0.147
r = 0.690
R² = 0.565
p-value 0.058
d
SPLEEN
LIVER
rank - % CFU reduction
rank - epitopes identified
r = 0.614
R² = 0.377
p-value 0.106
r = 0.602
R² = 0.362
p-value 0.115

Figure 5

a

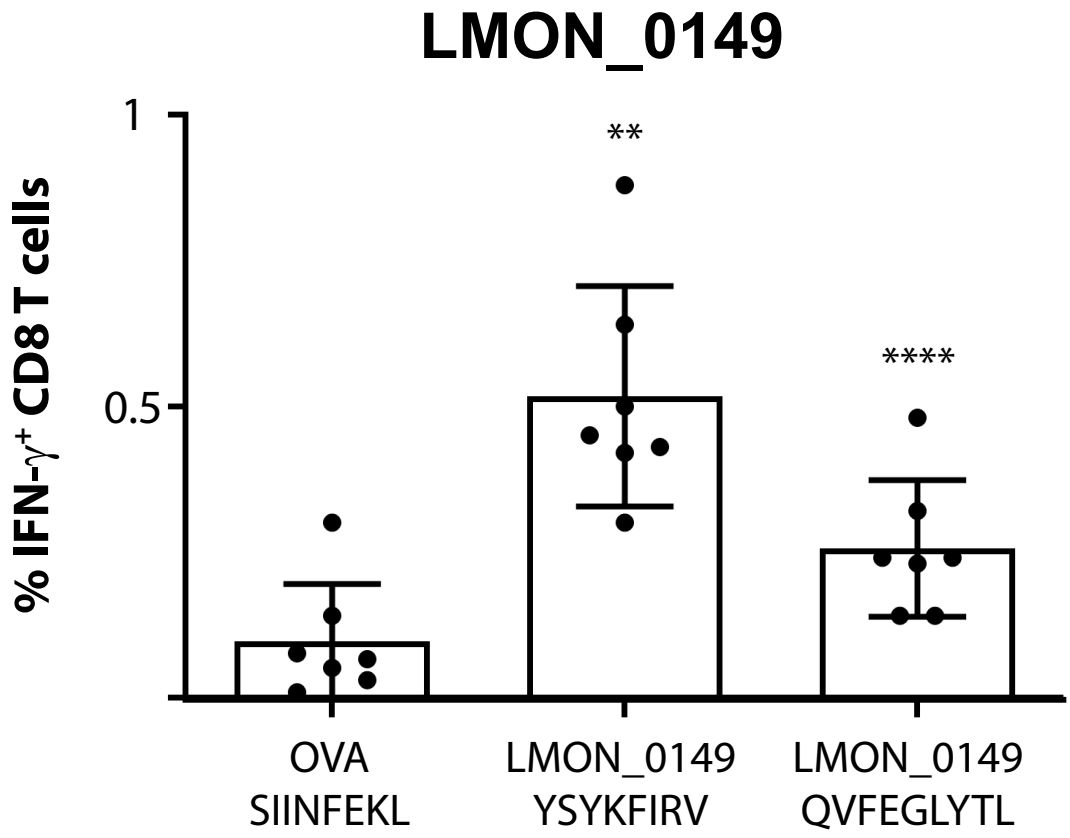
LMON_0149
% IFN-γ+ CD8 T cells
1
0.5
**
****
OVA SIINFEKL
LMON_0149 YSYKFIRV
LMON_0149 QVFEGLYTL

b

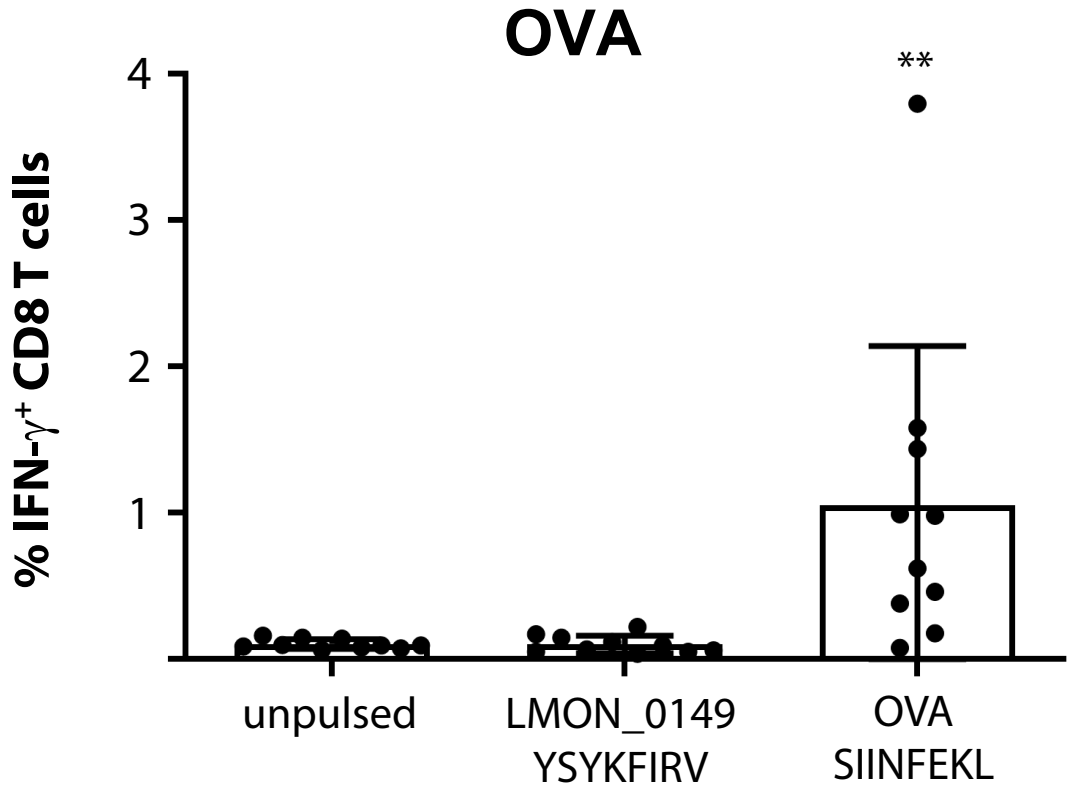
OVA
% IFN-γ+ CD8 T cells
4
3
2
1
**
unpulsed
LMON_0149 YSYKFIRV
OVA SIINFEKL